UCLouvain

AGRO LOUVAIN

Faculté des bioingénieurs

Quantification and characterization of Belgian cereals root system architecture and hydraulic architecture

Model-based approach

Auteur : Pierre Huljev
Promoteur : Guillaume Lobet (UCL/ELI/ELIA)
Lecteurs: Xavier Draye (UCL/ELI/ELIA)
Dominique Mingeot (CRA-W)
Année académique 2023-2024
Mémoire de fin d'études présenté en vue de l'obtention du diplôme de Bioingénieur : Sciences Agronomiques

Acknowledgements

First of all, I would like to thank Guillaume Lobet for introducing to root systems in Bac 1 and for having accompanied me throughout the year, always being available and open to discussion. Thank you for providing me with the foundations I needed to finalise this work.

I also want to thank Xavier Draye and Dominique Mingeot for agreeing to being in the jury of this master thesis.

I would like to thank the whole PEPA laboratory, especially Thomas Dagbert for his rhizotron and columns tutorial and his patience in sewing the 27 pieces of fabric one by one so that I could make these rhizotrons, which took a long time to make.

I'd like to thank Marco D'Agostino for helping me compile the MARSHAL model and for taking the time to proofread my dissertation. I owe you one hell of a drink.

I'd like to thank my family and close friends for supporting me all year and for trying to understand my subject, without much success, when in the end I spent most of my time doing scans.

I'd also like to thank the Cercle Industriel, the OCN and all my student friends who have been with me for these six long years and helped me get to where I am now.

CONTENTS

LIST OF FIGURES

LIST OF TABLES

LIST OF ABBREVIATIONS

- **RSA** : Root System Architecture
- **SCD** : Steep Cheap Deep
- **RCA** : Root Cortical Aerenchyma
- **FSPM** : Functionnal Structural Plant Models
- **RSML** : Root System Markup Language
- **CSV** : Comma Separated Values
- **ISRR** : International Society for Root Research
- **MARSHAL** : MAize Root System Hydraulic Architecture Solver
- **SUF** : Standard Uptake Fraction
- **RSHA** : Root System Hydraulic Architecture
- **HA** : Hydraulic Architecture
- **IQR** : Interquartile Range

INTRODUCTION

The development of a sustainable agricultural model represents a significant challenge for contemporary society. The agricultural practices derived from the Green Revolution of the 1960s are now demonstrating their limitations, thereby necessitating the exploration of new paradigms to address the emerging issues, such as the increasing frequency of droughts associated with climate change. The global agricultural sector is confronted with a multitude of challenges, including mounting pressure on arable land, declining soil quality, escalating costs of fertilizers and energy, and the detrimental effects of climate change (Ndour et al., 2017; Leitner et al., 2010).

Drought remains a significant constraint to agricultural production, affecting both developed and developing countries. There is considerable genotypic variation in root traits, which influence water acquisition and yield performance under water-limited conditions, across various crops. For plant breeders, developing cultivars with enhanced drought tolerance represents a viable strategy to address the challenge of emerging drought episodes. This approach is particularly crucial for subsistence crops in emerging economies, where populations depend heavily on the crops' effective adaptive capacities for their livelihood and survival (Lynch et al., 2014; Sultan et al., 2013).

Root systems are optimal candidates for the development of novel drought-tolerant cultivars due to their critical role in water uptake and their phenotypic plasticity, which enables them to adapt to varying environmental conditions. In light of the growing global population, it is imperative to enhance the efficiency of plant water and nutrient use in order to meet the rising demand for food. Plant productivity is influenced by a multitude of environmental factors, including radiation interception and the availability of water and nutrients in the soil. It is therefore imperative to gain a fundamental understanding of the processes governing plant growth if improvements are to be made to cropping systems and cultivars, particularly in environments where resources are limited (Leitner et al., 2010; Wasson et al., 2012).

CHAPTER 1

STATE OF THE ART

1.1 Root System Architecture

Root system architecture (RSA) describes the spatial distribution of the root system which is also the specific formation of root axes in the soil or substrate in which the plant grows (Roychoudhry and Kepinski, 2021).

RSA are defined by macroscopic (e.g.: length, angle of growth, number of axis) and microscopic (e.g.: diameter) parameters. The organisation of the RSA is critical for the plant's ability to absorb water and nutrients distributed heterogeneously within the soil (Roychoudhry and Kepinski, 2021). Water and nutrients regulate the formation of lateral and adventitious roots, but also the root growth to create a shallower or deeper root system (Del Bianco and Kepinski, 2018). While nutrients are often more abundant in the superficial layers of the soil, water can often only be found in the deeper layers, especially during drought (Del Bianco and Kepinski, 2018).

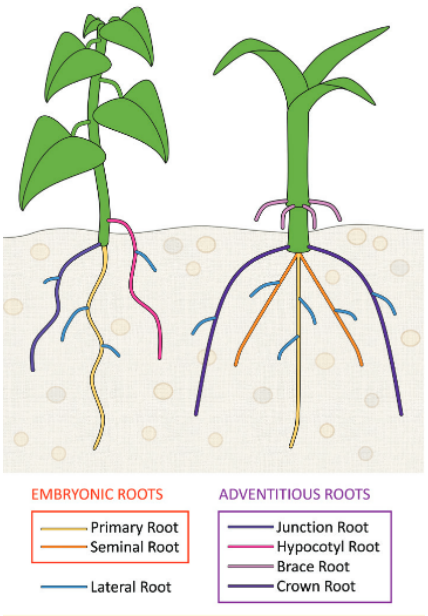

Figure 1.1: Different types of plant root (Del Bianco and Kepinski, 2018)

The root growth's plant regulator is auxin. The pivotal role of auxin is to regulate various aspects of root growth and development, including the initiation and elongation

of primary roots, lateral roots, and root hairs (Roychoudhry and Kepinski, 2021).

The interdependent relationship between the shoot, which is any plant stem together with its appendages, and roots is characterized by a mutual exchange of nutrients and water. The shoot supplies carbohydrates to the roots, while the roots provide water and nutrients to the shoot. The aforementioned equilibrium is subject to variation on a species-specific level. As demonstrated by Boote (1976), C4 plants exhibit a higher shoot-to-root ratio than C3 plants, while temperate legumes display a higher ratio than temperate grasses. In order to achieve optimal crop production, a smaller root system may be advantageous if it is capable of adequately supplying water and nutrients. Conversely, a larger root system could be beneficial in rapidly changing environmental conditions (Sheng and Hunt, 1991).

1.1.1 Root types

The root system of the monocotyledones is composed of many different type of roots, which can differ in origin, anatomy and fuction (Del Bianco and Kepinski, 2018). These types can be seen on the Figure 1.1.

Primary and Seminal roots

First there is the primary root originally from the embryon and the first to emerge upon germination, anchoring the new seedling to the ground and supplying initial nutrients. Secondly there are the seminal roots, which come from the extra embryonic root primordia. For the monocots, primary and seminal roots are important in the first stages of development (Del Bianco and Kepinski, 2018).

Adventitious roots

Adventitious roots, which do not come from any non-root tissue (Steffens and Rasmussen, 2016), appear later in the development so that they can constitute the majority of the root system for the cereal crops. In fact, like most monocots, cereal crops' root systems rely almost exclusively of adventitious roots (Steffens and Rasmussen, 2016). Ecologically, adventitious roots are important in many environments (coastal regions, estuaries and river flood plains) and stresses (biotic and abiotic) (Steffens and Rasmussen, 2016).

1.1.2 The ISRR nomenclature

Ever since humans discovered plant roots, they have tried to describe them to others by assigning descriptive names based on their origin site, apparent morphological function, presumed physiological function, and anatomical location (Zobel and Waisel, 2009).

In 1996, the International Society for Root Research (ISRR), which aims to promote cooperation and communication among root researchers globally, proposed a universal root taxonomic nomenclature (Zobel and Waisel, 2009). The outcomes of these discussions were summarized by (Schnepf et al., 2018):

1. **Tap root** is the first root that emerges from the seed.
2. **Lateral roots** can be caracterised as, on the one hand, first-order laterals that are any roots that branch from the tap root, basal roots or shoot-borne roots and, on the other hand, second order laterals that are lateral branches from first-order laterals.
3. **Basal roots** emerge from the the hypocotyl or mesocotyl.
4. **Shoot-borne roots** emerge from shoot tissue.

In monocotyledonous plants, all root types (1)–(4) can be observed, whereas in dicotyledonous plants, only root types (1)–(3) are present.

1.1.3 Cereals studied

Cereals are monocotyledones from the Poacea family. Their typical rootsystem can be seen on the Figure 1.2

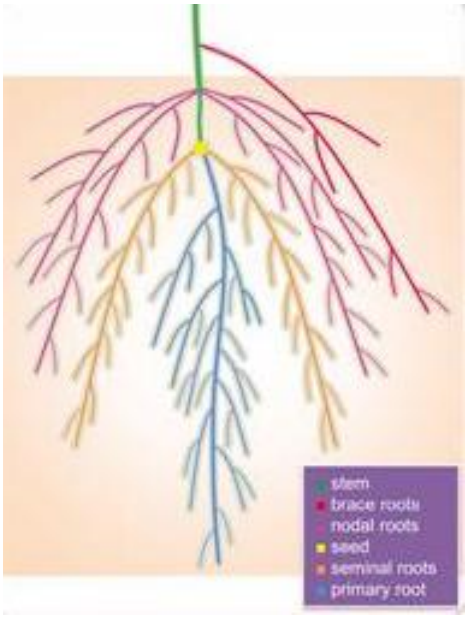

Figure 1.2: Graminea's rootsystem illustration (Correa et al., 2019)

Rye (*Secale Cereale*)

Rye scientifically known as *Secale cereale L.* is mainly a European cereal with about 75% of the global production growing in Russia, Belarus, Poland, Germany, and Ukraine. Its popularity is mainly due to its higher tolerance to abiotic stresses, such as drought, nitrogen deficiency, and high concentrations of aluminium, zinc, sodium, and acidity then wheat (Geiger and Miedaner, 2009).

Rye is closely related to wheat (*Triticum aestivum L.*) and has more properties that wheat lacks such as early spring vigour, its high water use efficiency an its high phytomass productivity (Sheng and Hunt, 1991).

Rye is capable of producing yields under conditions of extreme climatic stress, including low rainfall and low temperatures, which render other cereals unable to do so. Furthermore, rye demonstrates tolerance to poor soil conditions and exhibits exceptional zinc efficiency. Furthermore, rye is regarded as requiring minimal input in terms of fertilizers and pesticides, which makes it an ecologically and economically viable option for specific regions (Dreyer, 2018).

Oat (*Avena Sativa*)

The root system of oat, scientifically known as *Avena Sativa*, exhibits unique characteristics that contribute to its growth, nutrient uptake, and overall performance. Oat are recognized for their powerful root system, capable of absorbing hardly soluble nutrients, making them valuable crops in crop rotations (Eremina, 2021). Oat is thus a key plant in agricultural systems, particularly in enhancing soil fertility and nutrient cycling but also via intercropping with other species such as alfalfa and smooth brome as showed in the study led by Liu (2023). In fact, oat showed an increased in fine root density, which enhances water and nutrient utilization efficiency.

A comparative study led by Martin and Field (1987) between wild oat and wheat showed that wild oat exhibit more aggressive root systems. Moreover oat show prolific crown root development, potentially leading to better nutrient absorption and shoot growth compared to wheat (Martin and Field, 1987, 1988). Oat is also well adapted to marginal soils and requires minimum water and nutrients to produce biomass (Khan, 2019).

Spelt (*Triticum Spelta*)

Spelt is one of the oldest wheat subspecies, it has hardly changed at all since it was first domesticated. In the recent years, Spelt has gained an increasing attention due to its possibility for cultivation under extensive conditions (Żabiński, Andrzej and Sadowska,

Urszula, 2018). In fact, it is a robust crop with high levels of disease resistance making it suitable for organic farming (Wang et al., 2021). In addition, spelt has high amounts of essential nutrients, such as proteins, unsaturated fatty acids, carbohydrates, vitamins and bioelements, as well as fiber (Żabiński, Andrzej and Sadowska, Urszula, 2018). Its nutritional values defer from other cereals and especially wheat (Wang et al., 2021).

Spelt also has a higher tolerance to flooding (and thus to hypoxia) due to two specific traits (Burgos et al., 2001): a fast-growing coleoptile, which quickly reaches the soil surface, reducing the duration of hypoxia sensitivity, and the lower oxygen consumption between germination and emergence, leading to a better growth of the coleoptile under hypoxia.

The Fernando et al. (2021) study shows that spelt genotypes had the highest N uptake in comparison over the rest of the genotypes tested (wheat and emmer). Roots traits such as total root length, root volume, root biomass and root lentgh density were higher in spelt genotypes. This study also shows that the high plant N uptake is linked to more vigorous and robust root systems at anthesis and maturity.

Wang et al. (2021) concluded that spelt can be reliably produced in semi-arid regions (which are regions where the climate is characterised with insufficient rainfall in some years to support crops, and where evaporation often exceeds rainfall) using varieties developed in central Europe, but satisfactory yields and yield stability can only be achieved with supplementary irrigation and so spelt can be a precious crop with the rise of temperature in the future years.

1.2 Root water Uptake

1.2.1 Transpiration

The movement of water is driven by the difference of pressure between the roots and stomata. The main cause is the transpiration through stomata that creates a tension (negative pressure) that is sufficient enough to pump water through soil. For transpiration to take place in the xylem, a number of conditions must be met (Nagwa, 2024):

- The vessel must act as a capillary tube.
- The tubes must be free of gas or air bubbles.
- There must be no breaks in the xylem.

Transpiration rates are also influenced by 4 environmental parameters: light, temperature, humidity, and wind (Nagwa, 2024). In fact, daylight, high temperature, low

humidity and high wind speed, together or individually, will increase the rate of transpiration by increasing the potential difference between the stomata and the roots, thereby increasing water uptake from the soil.

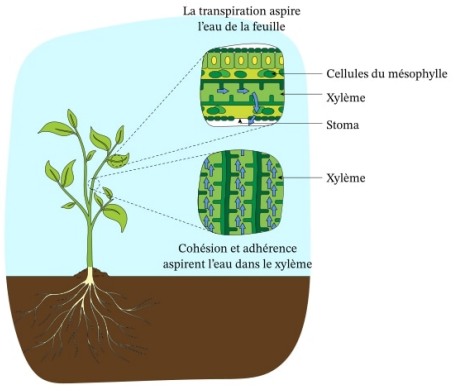

Figure 1.3: Cohesion Tension theory (Nagwa, 2024)

Transpiration can also be explain with a physics phenomena called the cohesion tension theory. This theory, proposed by Dixon (1894), illustrated by Figure 1.3, says that cohesion and adhesion of water in the vessel element help water move up the vessel without breaking under tension. Adhesion occurs when water molecules are attracted to the walls of the vessel element, which has thick walls with lignin (a stiff substance). Cohesion occurs when water molecules are attracted to each other. This is due to hydrogen bonds, strong intermolecular force, which form between the partially negative oxygen of one molecule and the partially positive hydrogen of another molecule. As some water molecules move up the vessel element, they pull other water molecules with them. Water molecules move up the xylem (Nagwa, 2024).

For Lobet et al. (2014), quantifying the water uptake depends on 3 properties that are shown on the Figure 1.4:

- **(A) Spatial Geometry:** Essentially the way roots place themselves in the soil but also the number of roots, their lengths and their diameters.
- **(B) Hydraulic Architecture:** Corresponds to axial (orange lines) and radial (blue lines) hydraulic resistances of individual root segments (gray circles) and soil elements (brown circles)
- **(C) Distribution and amount of available soil water:** with whites squares indicating dry soil and blue squares wet soil.

This movement of water from the soil to the leaves can be expressed as a combination of a radial flow from the soil to the xylem vessels and an axial flow through the xylem.

Water flow along the xylem tubes has been shown to be accurately described by Poiseuille's law for water flow in a cylindrical tube (Frensch and Steudle, 1989). The axial flux of water Q_x $[m^3 s^{-1}]$ through xylem is then represented by:

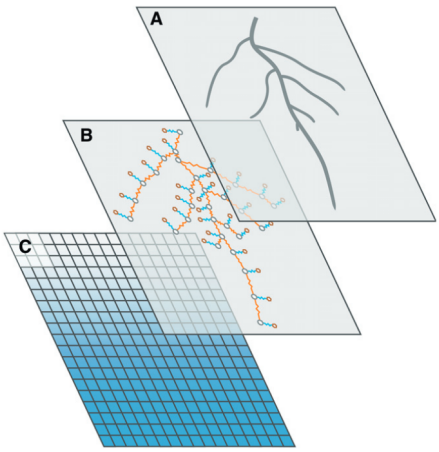

Figure 1.4: Properties of the soil-root system (Lobet et al., 2014)

$$Q_x = -K_x(\frac{p_r}{x} - \rho * g) \tag{1.1}$$

where p_r is the root fluid pressure inside the xylem tubes, x is the position along the root, rho is the density of water, g is the gravitational acceleration and K_x $[m^4 s^{-1} MPa^{-1}]$ is the axial conductance. K_x can be found using:

$$K_x = \sum_{i=1}^{N} \frac{\pi R_i^4}{8\mu} \tag{1.2}$$

where N is the number of xylem vessels, R_i is the radius of the i^th xylem file, and μ is the water dynamic viscosity. (Roose and Fowler, 2004).

For the radial flow and as seen on the Figure 1.5, the composite transport model proposed that water, in order to join the xylem from the soil, has to use 2 different parallel pathways: the apoplastic path and the cell-to-cell path (symplastic and transmembrane)(Kim et al., 2018; Steudle et al., 1993). Water using the cell to cell path can pass through either membranes or through plasmodesmata and cytosols. (Couvreur et al., 2018; Kim et al., 2018)

The water flow $J_w[m^3 m^{-2} s^{-1}]$ at the root surface can be expressed as:

$$J_w = k_r(\psi_{p,s} - \psi_{p,x} + \sigma_r(\psi_{o,s} - \psi_{p,x})) \tag{1.3}$$

where k_r $[m^3 m^{-2} s^{-1} MPa^{-1}]$ is the root radial conductivity (expressed here per root surface area), $\psi_{p,s}$ and $\psi_{p,x}$ correspond to the water pressure potential at the root surface and in xylem vessels, respectively, relative to the atmospheric pressure, σ_r is the effective root reflection coefficient (dimensionless; not to be confused with the reflection coefficient of a cell membrane), and $\psi_{o,s}$ and $\psi_{p,x}$ correspond to the osmotic potential at the root

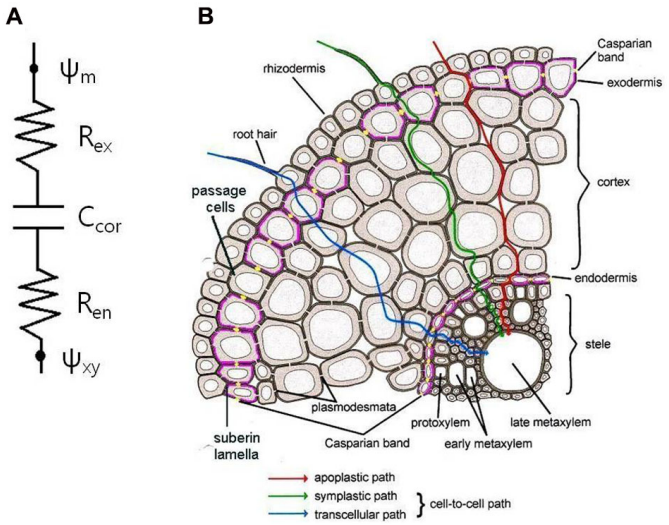

Figure 1.5: Radial Conductivity at the root-cross section scale (Kim et al., 2018)

surface and xylem vessels, respectively (Couvreur et al., 2018). Water channels (aquaporins) and plasmodesmata contribute to the regulation of k_r (Couvreur et al., 2018). A simplified version of this equation and for a given root surface can be expressed as:

$$J_w = 2\pi rh * K_r(\Delta\psi_p + \sigma_r \Delta\psi_o) \tag{1.4}$$

where $2\pi rh$ is the root surface (with r the radius of the root and h the height of the cross-section), $\Delta\psi_p$ is the difference in water pressure potential between the root surface and the xylem, and $\Delta\psi_o$ is the difference in osmotic potential between the root surface and at the xylem (Couvreur et al., 2018).

In conclusion, axial and radial conductance (K_z and k_r) are essential for modeling root system conductivity at the plant scale. They respectively quantify the transport and entry of water within the plant. These conductances can be combined to represent the overall root system conductance (K_{rs}) for the entire root system (Meunier et al., 2019).

1.3 The perfect rootsystem

A root ideotype is a conceptual framework employed in the fields of agriculture and plant biology to delineate an optimal model of a plant's root system, designed to optimise the efficiency of nutrient and water acquisition under specific environmental conditions.

In general, crop growth is frequently constrained by two mobile resources, water and nitrate, as well as two immobile resources, phosphorus and potassium. Steep Cheap and deep (SCD) is an ideotype proposed to optimize water and nitrogen uptake, whose main focus in on maize, although it can apply to other monocotyledonous crops and consists

in the integration of architectural, anatomical and physiological phenes that enhance the exploration of the deep soil (Lynch, 2013). SCD is based on some premises to develop its RSA:

1. The acquisition of soil resources is inextricably linked to the synchronisation of root foraging and resource availability in both temporal and spatial dimensions.
2. The availability of water and nitrogen are greater in deeper soil strata over the growing season in the majority of soils.
3. The effectiveness of root phenotypes for soil resource acquisition should consider both the benefits and costs of specific root traits.

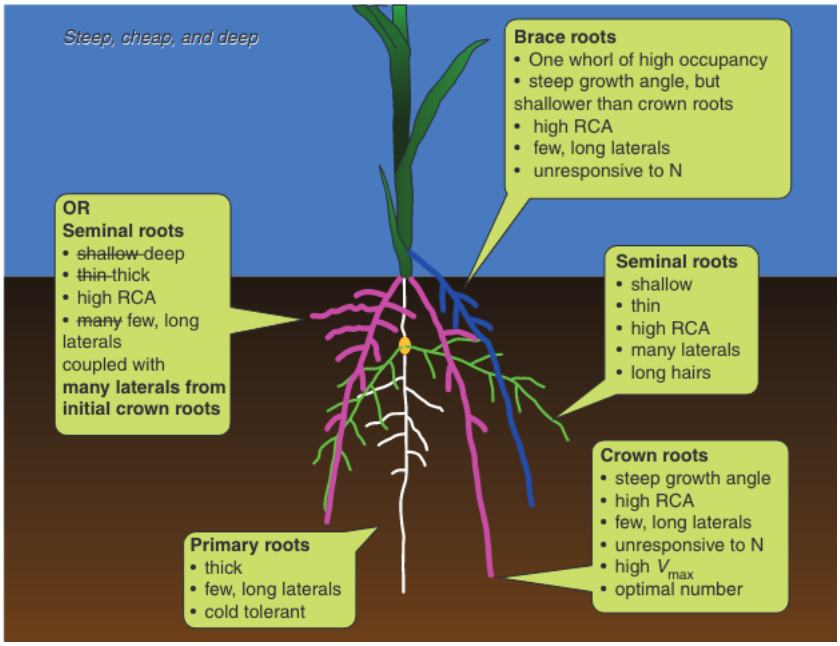

Figure 1.6: Ideotype for optimal acquisition of water and N for maize by Lynch (2013)

We can summarize the roots traits that are optimal in our case:

- **Large Diameter**: roots that have a large diameter have the capacity to penetrate hard soils and to reech their deeper part. As Thaler and Pagès (1998) considered that a root is a sink, the larger its diameter will be, the more the sink strength will be and thus the elongation rate will be larger as demonstrated by Pagès et al. (2010).
- **High Root Cortical Aerenchyma (RCA)**: RCA consists in converting living cortical tissue to air space to reduce nutrient and carbon costs. RCA is linked to the increase of N, P and K acquisition in low fertility soils (Postma and Lynch, 2011) and in more resistance to drought conditions (Zhu et al., 2010).

- **Steep Growth Angle**: The growth angle of axial roots exerts a significant influence on rooting depth in a range of crops, with steeper angles conferring a distinct advantage in terms of water acquisition during periods of drought. Roots with a steep angle of inclination are capable of effectively exploiting deep soil resources without compromising access to topsoil resources, as new root systems continuously pass through the topsoil during vegetative growth (Lynch, 2013).

- **Lateral Roots**: are metabolically more demanding per gram of tissue than axial roots and compete for internal resources, which may also result in a slowing of the elongation of the main root axis. Mobile resources are more efficiently captured by fewer, but longer, lateral roots that can explore larger soil volumes. Therefore, lateral root phenotypes optimised for water and nitrogen capture should be characterised by longer and more widely dispersed roots along the axial root system (Lynch, 2013).

But can this root ideotype be applied to our species under study? In fact the root systems of wheat, rice, barley, spelt, and oat are comparable to maize in terms of their fundamental structure but are smaller and produce multiple tillers, each of which generates roots. The number of tillers, like the crown root number in maize, should be optimized for resource capture. Due to their smaller size, these crops require rapid deep root development to prevent resource loss from leaching and their smaller size leads to more competition for mobile resources within the plant, making lateral root dispersion and cortical senescence potentially more beneficial. Since their roots are mostly in shallow soil, balancing topsoil and deep soil foraging is less crucial.

The Figure 1.6 summarises the ideal parameters for each type of root.

1.4 Modelling architecture and water flow

Modeling the development of the root system in relation to its environment represents a promising approach to enhance our understanding of the plant–soil system. Explicit three-dimensional models of the RSA provide insights into both the location of roots (affecting the soil–root transport of water and nutrients) and the structural properties of the root system (Pagès et al., 2014a).

Root architecture models, such as SimRoot (Lynch et al., 1997), RootBox (Leitner et al., 2010), RootTyp (Pagès et al., 2014b), ArchiSimple (Pagès et al., 2014a), OpenSimRoot (Postma et al., 2017), and CRootBox (Schnepf et al., 2018), simulate root systems using a limited set of traits as input parameters. The primary benefit of this approach is the capacity to generate a diverse array of contrasting root architectures, thereby facilitating the investigation of multiple variants with identical average traits (Passot et al.,

2019). In his article, Schnepf et al. (2018) summarized all the major root architecture models which can be view in the Table 1.1.

Model name	**Authors**	**Type of model**
ROOTMAP	Diggle (1988)	Root system
SimRoot	Lynch et al. (1997)	Root system
ArtRoot	Spek (1997)	Root system
GRAAL	Drouet and Pagès (2003)	Whole-plant structure and plant carbon flow
CRoot Typ	Pagès et al. (2004)	Root system
SPACSYS	Wu (2007)	Ecological model, RSA submodel
R-SWMS	Javaux et al. (2008)	Coupled soil and root system
RootBox	Leitner et al. (2010a)	Root system
PlaNet-Maize	Lobet et al. (2014)	Whole-plant structure and plant water flow
ArchiSimple	Pagès et al. (2014)	Root system
OpenSimRoot	Postma et al. (2017)	Coupled soil and root system

Table 1.1: Overview of major root architecture models (Schnepf et al., 2018)

In the context of root-related drought, Functional Structural Plant Models (FSPMs) are a particularly intriguing area of study due to their capacity to simulate the intricate processes of plant development, growth, and function at the cellular, tissue, and organ levels. These models establish a link between plant structure and physiological processes, which are driven by environmental factors. The effectiveness of these models is closely tied to advancements in phenotyping techniques (Ndour et al., 2017; Passot et al., 2019).

The application of FSPMs to crop root systems facilitates the comprehension of the influence of RSA on physiological processes. These models integrate a comprehensive portrayal of root architecture with functional attributes, including hydraulic parameters, which are pivotal for modeling soil-root interactions and water stress. Nevertheless, the acquisition of accurate hydraulic parameters can prove to be a challenging endeavor, frequently necessitating adaptations derived from existing literature (Ndour et al., 2017; Passot et al., 2019).

FSPMs related to water flow provide a comprehensive view of root water relations across space and time, integrating experimental data to model water dynamics in the root zone. This information, which is difficult to obtain experimentally, is essential for advancing our understanding of plant physiology. These models are of great importance for the comprehension of water availability and stress in plants (Ndour et al., 2017; Passot et al., 2019).

CHAPTER 2

OBJECTIVES

Rye, oat, and spelt are already utilized in our regions for both human and animal consumption. Given the likelihood of increased periods of drought due to global warming, it is crucial to understand the resilience of these species to such changes. In the absence of irrigation, it is essential to ascertain their ability to adapt and survive in the face of environmental shifts. Furthermore, the development of the root architecture of these cereals and its impact on the extraction of water from the soil have yet to be extensively studied. This master thesis is part of this approach and therefore focuses on modeling the root system of rye, oat, and spelt in order to identify their specific traits. The following objectives have been set:

1. **Characterize and quantify the root system of each species**. To achieve this objective, three varieties of each species will be studied and cultivated in both rhizotrons and columns. Subsequently, the scans of these architectures will be subjected to analyses.

2. **Identify any potential differences between these species**. This may be achieved through the use of statistical and visual analysis.

3. **Simulate the root systems architecture of these species**. The CRootBox model was selected for its user-friendly interface and intuitive design.

4. **Compute water flow and macroscopic parameters** with MARSHAL model.

In a more general sense, this research is part of a larger study that aims to gain a deeper understanding of the internal water flows within plants. The objective is to identify crop varieties and genetic traits that enhance resilience to frequent droughts, thereby facilitating varietal and genetic selection. It should be noted that this work is not intended to be a comprehensive study. Rather, it is a contribution to the broader research field of water flows within plants.

CHAPTER 3

MATERIALS AND METHODS

3.1 Genotypes selection

For each species under investigation, three distinct genotypes were selected on the basis of a seed proposal from Dominique Mingeot(CRA-W). The objective was to examine a number of genotypes in order to identify potential differences in their architectural characteristics. These genotypes were selected on the basis of their prevalence in Belgian agricultural systems.

The genotypes are listed in Table 3.1 together with the identifier assigned to them, which will subsequently be used to differentiate the samples. The identifier is comprised of two letters. The initial letter is a reference to the species and the second is associated to the variety of the plant.

Identifier	**Varieties**	**Species**	**Country of Obtention**	**Year**
AJ	Jacky	*Avena Sativa*	Germany	2023
AO	KWS Opaline	*Avena Sativa*	France	2019
AL	Lion	*Avena Sativa*	Germany	2018
SS	KWS Serafino	*Secale Cereale*	Germany	2017
ST	KWS Tayo	*Secale Cereale*	Germany	2018
SP	Poséidon	*Secale Cereale*	Germany	2019
EC	Cosmos	*Triticum Spelta*	Belgium	2000
ES	Sérénité	*Triticum Spelta*	Belgium	2015
EZ	Zollernspelz	*Triticum Spelta*	Germany	2006

Table 3.1: Selected Genotypes

3.2 Architectural measurements

In order to model the root architecture of the selected species, two types of experiment were conducted. The first employed rhizotrons, while the second used columns. Both experiments were conducted in the same greenhouses under identical conditions. At the conclusion of the experiments, roots in the early stages of cultivation were sampled.

3.2.1 Rhizotron

A rhizotron is a type of set-up that makes it possible to observe root development in two dimensions and to take precise measurements of root expansion rates and root architecture in general. (Graw-Hill, 2002)

The rhizotron has a basic structure consisting of a wooden plate with moss around it. This plate can then be filled with a substrate that can vary according to the researcher's choice. In order to prevent fungi from multiplying within the rhizotron, the lab chose to make the transition from filter paper (which is highly conducive to their development) to a piece of fabric designed to act as a barrier and prevent their growth. This method worked well in my experiment, as I did not see any fungus appear and interfere with the growth of my plants. Once the piece of fabric is in place, the set-up can be closed off by placing a plate of plexiglas which we can put behind the seed of the plant being studied can be placed. Putting the seed behind a transparent plate allows you to follow the plant's development over time. Watering, and therefore the supply of nutrients, takes place directly in the substrate, and the fabric is obviously permeable to these nutrients, allowing the roots to pick them up easily.

A diagram of the rhizotron set-up is shown in Figure 3.1. The diagram is inspired by the one used during the study of (Passot et al., 2016). Three rhizotrons measuring 60x20 cm were created for each species, making a total of 27 rhizotrons for the experiment as a whole. The experiment was carried out over four weeks (from 8th April to 8th (for spelt) and 13th (oat and rye) May)in the 'S.O.1' greenhouse at UCLouvain, where a temperate atmosphere was created to ensure optimum growth for cereals grown in our latitudes. The 27 rhizotrons were divided into three tanks of nine rhizotrons each, as shown in Figure 3.2. These rhizotrons are oriented downwards so that the roots grow along the Plexiglas plate and do not grow through the piece of fabric.

For the duration of the experiment, 50 ml of Hoagland's solution was added twice a week on Mondays and Fridays. This solution was chosen because it provides the maximum amount of nutrients necessary for good plant growth. Details of Hoagland's composition can be found in the Appendix A.1. This frequency of watering allows each plant to develop without any stress. On a regular basis, the roots are traced to measure growth

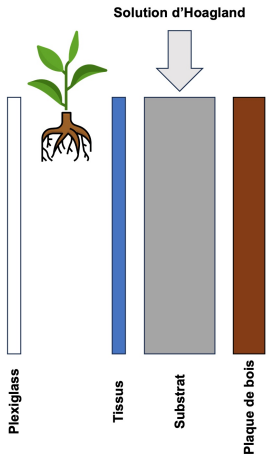

Figure 3.1: Rhizotron diagram

parameters. An example of one of these tracings can also be found in the Appendix B.1. At the end of the experiment, the above-ground parts were collected and placed in an oven at 60°C for 72 hours. This allowed the water to evaporate, enabling the subsequent weighing and measurement of the dry weight of the above-ground parts.

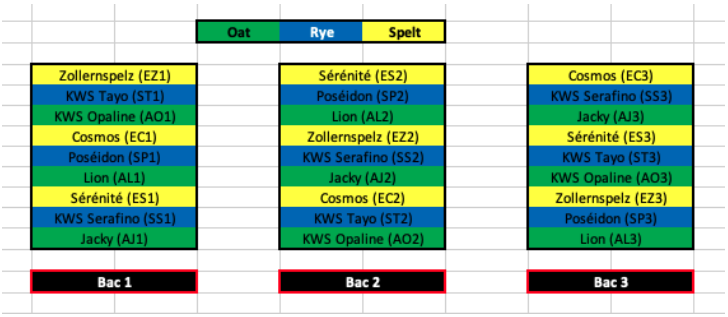

Figure 3.2: Rhizotrons experiment diagram

Figure 3.3: Rhizotrons at the beginning of the experiment

3.2.2 Columns

Another part of the experiment involved growing the same cereals in columns. The principle here was to carry out a longer experiment in order to allow the root network to develop and also to be able to check the aerial parts and the different aerial development phases of the plant and relate them to the root development. 27 columns were therefore arranged according to the figure 3.4.

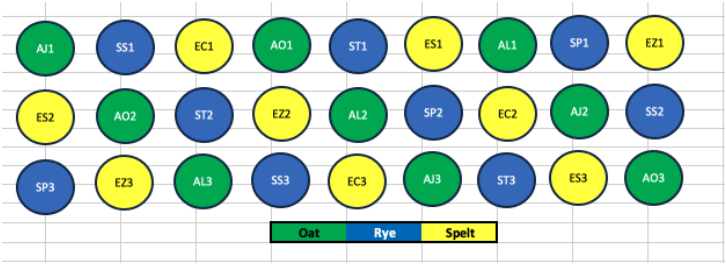

Figure 3.4: Columns experiment diagram

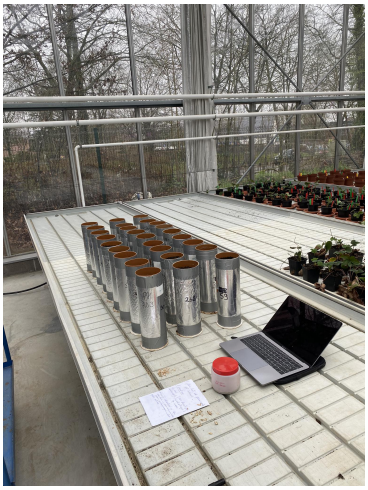

Figure 3.5: Columns at the beginning of the experiment

The phenological stages of the plant were monitored using the **BBCH** scale (Meier et al., 2009). This is inspired by the Zadok code and involves giving each plant a two-digit code that will change over time. This code uses a decimal system subdivided into main and secondary growth stages. The main stages are described from 0 to 9 and are completed by secondary stages ranging from 0 to 9 within a main stage. The result is a 2-digit code. They can be described as follows:

0. Germination, emergence
1. Leaf development
2. Tillering
3. Elongation of the main stem
4. Swelling of the ear or panicle, bolting
5. Inflorescence emergence or heading
6. Flowering, anthesis
7. Seed development
8. Maturation of seeds
9. Senescence

In this experiment, in the same way as for rhizotrons, three columns will be tested per genotype, bringing the total number of columns to 27. The substrate here is fertiliser, so that the plants have all the nutrients they need to grow right from the start. Therefore,

a weekly watering with tap water was enough to allow the plants to grow. 1320g of this fertiliser was put in each column and the equivalent of 75ml of water was put in every Wednesday **from Monday 26th February to Monday 8th April 2024**. Three seeds were sown to ensure that at least one would germinate. Two days later the plants with the lowest development stage (see BBCH scale) were removed.

Similarly to the rhizotrons, the above-ground parts were placed in the oven under the same conditions (see Section 3.2.1)and will be weighed to measure the dry weight of each.

3.3 Root image analysis

All root samples were scanned using the Epson Perfection V850 Pro scanner from the PEPA laboratory. The scans were made using the configuration available in Appendix C.1.

All the measurements carried out on the root samples scans were made using Smartroot (Lobet et al. (2011)). SmartRoot is a platform-independent image analysis software package (Windows, MacOS, Linux) implemented as a plugin for ImageJ that enables the quantification of growth and complex root architecture. This quantification is carried out by tracing images of root system samples. The roots are therefore a sequence of nodes that are linked together. From these nodes we can find parameters such as length, diameter and lateral density for example.

Figure 3.6: SmartRoot layout

Image analysis software can be divided into three categories (Lobet et al., 2011):

- **Manual methods:** where the user draws the skeleton of the root system using freehand tools. These methods give accurate estimations of the traits and are often

the only option for complex root systems. However, they are highly time-consuming.

- **Automated methods:** which are highly specific case adapted to the software but they are very fast and require very little work.
- **Semi automated methods:** that use skeletonization algorithms to facilitate and accelerate image analysis, with the user intervening to correct and direct the algorithms.

In our case, Smartroot has been designed to trace roots in a semi-automated way. The software combines a highly intuitive user interface with a new tracing algorithm and supports sampling-based image processing (Lobet et al., 2011).

The file containing the root trace is saved using the Root System Markup Language (RSML) format. RSML is an XML-based standard developed to facilitate the standardization of root imaging and phenotyping processes in plant research. RSML was created to streamline the sharing of root architecture data (including information on geometry, and relative position within the system) between different software platforms, enabling seamless data transfer and promoting collaboration within the scientific community (Yasrab et al., 2019). This standardized format has been instrumental in enhancing research exchanges and establishing a common ground for root system data analysis and modeling (Lobet et al., 2015). Researchers have leveraged RSML to develop automated root analysis pipelines, deep learning models for root phenotyping, and image analysis tools for root trait assessment (Yasrab et al., 2020; Lobet et al., 2017, 2011). The adoption of RSML has facilitated the accurate quantification and evaluation of root system architectures, contributing to a deeper understanding of plant root dynamics and responses to environmental stimuli (Lobet et al., 2011).

Once the RSML files have been generated for each root sample, they can be exported to a CSV file containing comprehensive root information. This CSV file will include the necessary parameters for subsequent modeling, and it is with these files that descriptive analysis and statistical inference will be conducted. For each repetition of plant variety, we have a CSV file that contains all the information needed for later analysis. The contents of these files are as follows:

- Columns: Identifier_Repetition_global.csv (e.g.: AJ1_global.csv)
- Rhizotrons: Identifier_Repetition_tot.csv (e.g.: AJ1_tot.csv)

3.4 Rootsystem simulations

3.4.1 Crootbox

CRootBox is a structural-functional modeling framework for root systems that serves as a powerful tool in plant root research. Developed as a successor and C++ porting of the Matlab-based Root-Box model (Leitner et al., 2010), its structure changed from an L-systems to an object oriented design where each root is an object (Schnepf et al., 2018). CRootBox is designed to simulate realistic root systems by taking root architecture parameters as model input (Schnepf et al., 2018).

As presented earlier in the State of the Art (see Section 1.1.2), CRootBox uses the nomenclature of the ISRR to distinguish the physiological types of roots (Schnepf et al., 2018). Since cereals are indeed monocotyledonous, all root types will be found. To model a monocotyledonous plant, all input parameters and their units are summarized in Table 3.2. These parameters represent the emergence of basal roots (firstB, delayB, and maxB) as well as shoot-borne roots (firstS, delayS, ns, and dzS). The planting depth of the seed is specified by the parameter depth, with the hypocotyl assumed to be situated between the soil surface and the planting depth. The mesocotyl is located between half the planting depth and the seed. Basal roots emerge at the seed, while the first shoot-borne root emerges above the mesocotyl. (Schnepf et al., 2018).

Having established and validated the parameters for the plant type, we now need to determine the model parameters for each root type. Table 3.3 provides a comprehensive list of these model parameters along with their respective units.

No dataset available in CRootBox contains information on parameter values for the studied species. Additionally, due to the limited literature on all the studied species, the choice was to use parameters identified for wheat (*Triticum aestivum*), which is the species most similar to our studied species. More details on these parameter can be found in Appendix C of the CRootBox article (Schnepf et al., 2018) and are based on the study by (Bingham and Wu, 2011).

Table 3.2: List of plant parameters needed for the root architecture development of dicotyledonous and monocotyledonous plants

Description	**Parameter name**	**Unit**	**Plant type**
Planting depth	depth	cm	Dicot and monocot
First emergence of basal roots	firstB	day	Dicot and monocot

Table 3.2: (continued)

Description	**Parameter name**	**Unit**	**Plant type**
Time period between basal roots	delayB	day	Dicot and monocot
Maximal number of basal roots	maxB	1	Dicot and monocot
First occurrence of shoot-borne roots	firstS	day	Monocot
Time period between shoot-borne roots	delayS	day	Monocot
Number of shoot-borne roots per root crown	nS	1	Monocot
Distance between root crowns along the shoot	dzS	cm	Monocot

Table 3.3: Complete list of parameters used by CRootBox for each root type

Description	**Parameter name**	**Units**
Root radius	a	cm
Initial elongation rate	r	cm d^{-1}
Insertion angle	θ	rad
Length of basal zone	l_a	cm
Length of apical zone	l_b	cm
Length between lateral branches	l_n	cm
Maximal root length	l_{max}	cm
Tropism type	type	{0,1,2,3}[1]
Number of trials (tropism strength)	N	1
Standard deviation of random angular change	σ	cm^{-1}
Root successor types	successor	[type, probability; ...]
Name of the root type	name	String
Root colour	colour	RGB
Resolution along root axis	dx	cm
Root life time	rlt	day
Type of root elongation	gf	{1,2}[2]

Table 3.3: (continued)

Description	Parameter name	Units
Scale elongation	se	Function[3]
Scale branching probability	sbp	Function[3]
Scale branching angle	sa	Function[3]

CRootBox thus estimates the evolution of a RSA based on several major processes. Each of these processes is quantified using the input parameters presented in the tables above. They are detailed as follows:

1. **Growth and decay**: Each root elongates as long as its age is less than its life-time **rlt**. CRootBox is highly flexible and allows the user to implement their own function for root growth. However, two functions are already included: a negative exponential growth function and a linear growth function. The length of the root at a certain time t is given by:

$$l_{lin}(t) = min(l_{max}, r * t) \tag{3.1}$$

$$l_{exp}(t) = l_{max}(1 - \exp^{-\frac{rt}{l_{max}}}) \tag{3.2}$$

where l_{max} is the maximal length a root may reach and r is the initial growth rate. In the linear growth function, r is a fixed value. In contrast to the negative exponential growth function, where r is a function of root age and decreases over time (Schnepf et al., 2018).

2. **Radial Growth**: In CRootBox, the root radius is set to be a fixed value for each root type. But Secondary root growth can be done a posteriori using a function based on root age, the root radius is then computed as a 'pipe' model where the number of laterals on a parent root can affect its diameter (Schnepf et al., 2018). But in our case, for monocotyledonous species, the roots don't undergo radial growth (Pagès et al., 2014a).

3. **Branching**: For each root, basal, branching, and apical zones are distinguished. The laterals are only created when the basal and apical have been developed fully. They appear at a regular inter-branching distance given by the parameter l_n, with a maximal number of lateral roots Nob and with an insertion angle θ between the parent root and the new lateral root (Meunier et al., 2019). The maximal root length l_{max} for a given root is:

$$l_{max} = l_a + l_b + (Nob - 1)l_n \tag{3.3}$$

where l_a is the length of the apical zone, l_b is the length of the basal zone.

4. **Random and directed changes in root growth direction**: In CRootBox, after each distance dx, the root tip orientation is randomly changed to represent soil tortuosity. This random angular change is scaled by the root segment length dx and follows a normal distribution with zero mean and standard deviation σ. This approach ensures that the root system trajectories are independent of the spatial resolution along the root axes. The standard deviation then becomes:

$$\sigma_{dx} = \sqrt{dx} * \sigma \tag{3.4}$$

where σ describes the change in growth direction per unit (cm) of root length (Schnepf et al., 2018).

At the end of the modeling process, a txt file is generated containing all the segments that form the entire root architecture. Each segment includes a length, a radius, and the time at which the segment appears. By loading this file, images can be displayed as shown in Figure 3.7.

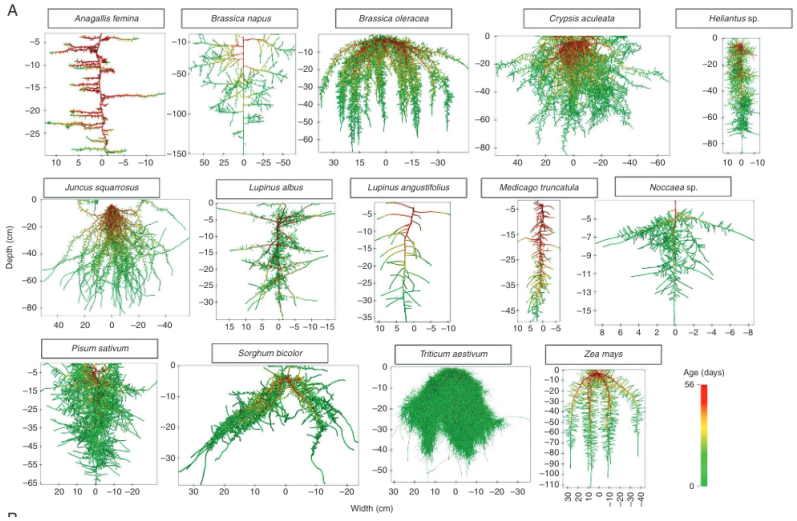

Figure 3.7: Root images obtained with CRooBox (Schnepf et al., 2018)

3.4.2 MARSHAL

MARSHAL (MAize Root System Hydraulic Architecture soLver) is capable of combining the root architecture model CRootBox Schnepf et al. (2018), the model of water flow in the Root sytem hydraulic architecture (RSHA) of Meunier et al. (2017), and the model to compute the macroscopic parameters of Couvreur et al. (2012). MARSHAL is available as an R package. It is available through two platforms: an RMarkdown pipeline for batch analysis and a Shiny web application for manual analysis (Meunier et al., 2019).

The water flow model included in MARSHAL calculates water flow in hydraulic architecture (HA) based on user-defined boundary conditions, including stem water potential

Table 3.4: Root, root system and root system macroscopic parameters. L = length, P = pressure, T = time. Actual model units are cm (L), hPa (P) and day (T) (Meunier et al., 2019).

Name	Dimension	Description
Root-type parameters		
v	L T^{-1}	Initial elongation rate
l_{max}	L	Maximal single root length
r	L	Root radius
θ	-	Insertion angle
d_{inter}	L	Inter-branching distance
n_{ob}	-	Maximal number of lateral roots
k_r	L T^{-1} P^{-1}	Root radial conductivity
k_x	L^4 T^{-1} P^{-1}	Root axial conductance
$agetr, k_x$	T	Transition ages for root axial conductance
Root system parameters		
N_{max}	-	Maximal number of main axes
t	T	Starting time of crown or brace root development
z_{cr} and z_{br}	L	Vertical position of crown and brace root development
Root system macroscopic parameters		
K_{rs}	L^4 T^{-1} P^{-1}	Root system conductance
z_{SUF}	L	Depth of Standard Uptake Fraction
V_{rs}	L^3	Root system volume
V_{ch}	L^3	Convex hull volume

(ψ_{collar}) and soil-root interface water potentials (ψ_{sr}). It provides the xylem water potential (ψ_x) at the basal end of each root segment, considering root radial hydraulic conductivity (k_r) and specific axial hydraulic conductance (K_x). The water potential vector (ψ_x) varies with root type and segment age (Meunier et al., 2017). The hydraulic parameters are listed in Table 3.4. The solution involves solving the equation:

$$\psi_x = a^{-1} \cdot b \tag{3.5}$$

where "a" is a matrix $[N_{seg} \times N_{seg}]$ and "b" is a vector $[N_{seg} \times 1]$, both derived from the root system architecture and properties, and the radial water flow in each segment $J_{r,i}$ with the equation:

$$J_{r,i} = 2 \cdot \kappa_i \cdot \tanh\left(\frac{\tau_i l_i}{2}\right) \cdot \left(\Psi_{sr} - \frac{\Psi_{x,-1,i} + \Psi_{x,i}}{2}\right) \tag{3.6}$$

where κ_i (defined as $\sqrt{2} \cdot \pi \cdot r_i \cdot k_{r,i} \cdot k_{x,i}$) and τ_i (defined as $\frac{\sqrt{2} \cdot \pi \cdot r_i \cdot k_{r,i}}{k_{x,i}}$) are hydraulic-specific root segment properties, $\Psi_{x-1,i}$ is the water potential at the proximal end of each segment (Equation (3.5)) and l_i the root segment length (Meunier et al., 2017, 2019)

Once equations (3.5) and (3.6) are solved, MARSHAL can then calculate all the macroscopic parameters inspired by Couvreur et al. (2012): the root system conductance K_{rs} (from soil-root interfaces to xylem vessels at the plant collar) and the Standard Uptake Fractions (SUF:the relative contribution of each root segment to the total water uptake under homogeneous soil water potential conditions) (Meunier et al., 2019). The calculations are performed according to the equations:

$$K_{rs} = \frac{T_{act}}{\Psi_{sr} - \Psi_{collar}} \tag{3.7}$$

and

$$SUF_i = \frac{J_{r,i}}{T_{act}} \tag{3.8}$$

where T_{act} is actually the sum of all the water flows from segments i:

$$T_{act} = \sum_{i=1}^{N_{seg}} J_{r,i} \tag{3.9}$$

SUF_i is then used to calculate z_{SUF}, which is the average uptake depth as the weighted mean of the depths of root water uptake (Meunier et al., 2019) with:

$$z_{SUF} = \sum_{i=1}^{N_{seg}} z_i \cdot SUF_i \tag{3.10}$$

where z_i is i^{th} root segment depth (Meunier et al., 2019).

Additionally, during each run of the model, MARSHAL computes various geometrical properties of the root system. These include the convex hull volume of the root system (V_ch), which is the volume of the smallest convex shape that fully encloses the root system; the root length density profile (RLD), which measures the amount of root length per unit volume of soil; and the total root system volume (V_rs), calculated as the sum of the volumes of all individual root segments (Meunier et al., 2019).

The Figure 3.8 shows the overall model workflow of MARSHAL. Initially, the user inputs model parameters related to the RSA, hydraulics, and environmental conditions. MARSHAL then calculates the HA, the macroscopic properties and the water flow. The resulting RSHA can be visualized in 3D or through plots. Finally, root system metrics and RSHA can be exported in standard formats for further applications (RSML, CSV, VTP and RSWMS) (Meunier et al., 2019).

The distribution of axial conductance and radial conductivity is shown in Figure 3.9 and Figure 3.10 for main axes and branch roots, respectively. The data demonstrate that axial conductance increases while radial conductivity decreases with increasing dis-

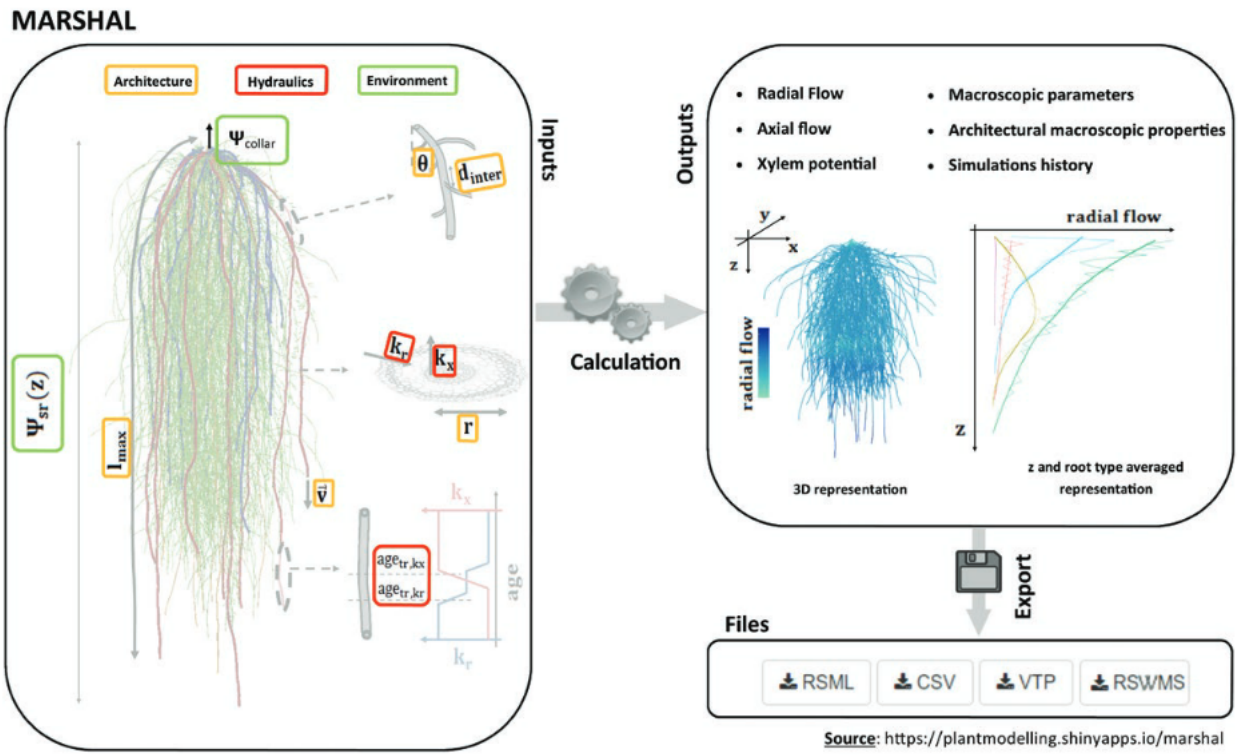

Figure 3.8: Schematics of MARSHAL workflow (Meunier et al., 2019)

tance from the root tip and, consequently, with increasing root age. Furthermore, it is evident that these processes occur in a synchronous manner, with the root transitioning from an absorptive to a transporting function with respect to water. This phenomenon can be attributed to the maturation of the root as it ages, which results in an increased hydrophobic tissue. In conclusion, the maturation of root tissues is accompanied by a decrease in radial conductivity of approximately one order of magnitude, while axial conductance increases by approximately three orders of magnitude (Doussan, 1998). This distribution will be employed in subsequent MARSHAL simulations.

Moreover, the water soil potential is described in the Table 3.5. The instrument is employed for the purpose of ascertaining the water content of the soil. Two scenarios are presented: one representing a dry environment and the other a wet environment. The values for these scenarios are derived from the MARSHAL pipeline data set referenced in Heymans et al. (2018). Given the aforementioned parameters, simulations can be readily conducted with any type of roof system.

Depth (cm)	Psi Humid (hPa)	Psi Dry (hPa)
0	-15000	-15000
-40	-300	-7000
-80	-300	-7000
-120	-300	-7000

Table 3.5: Water soil potential in fuction of depth

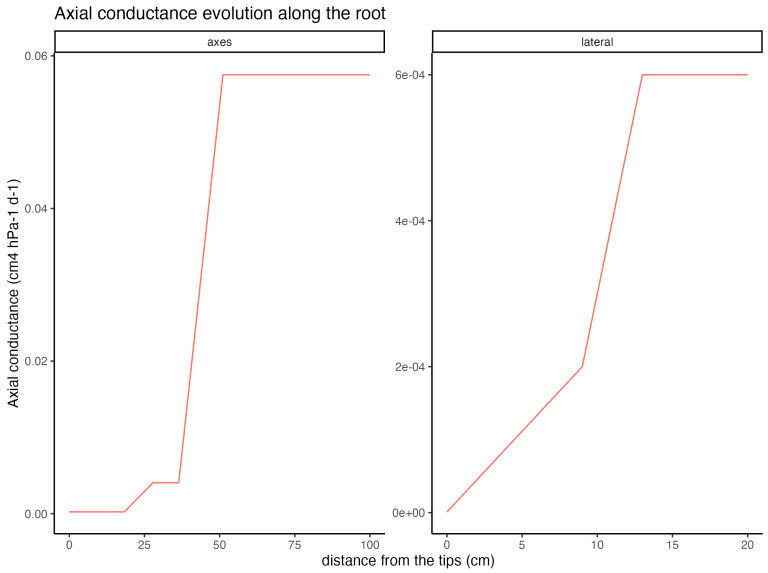

Figure 3.9: Kx evolution along the root for laterals and axes (Doussan, 1998)

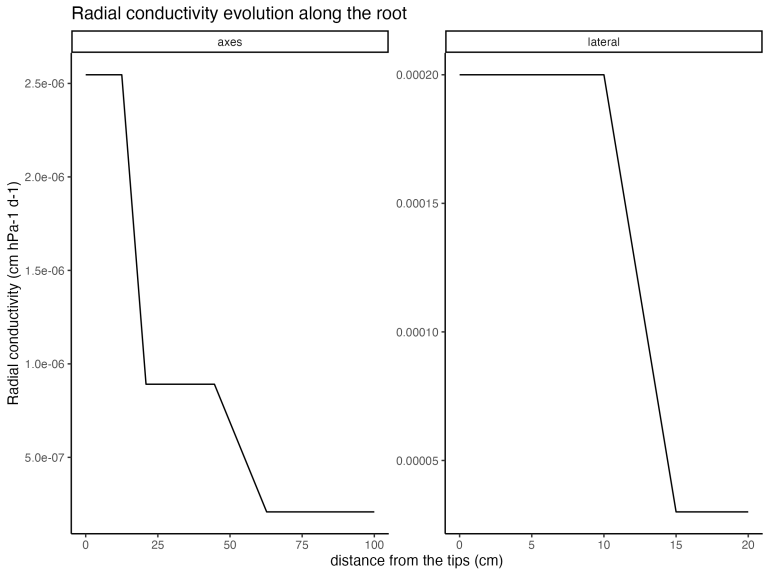

Figure 3.10: Kx evolution along the root for laterals and axes (Doussan, 1998)

3.5 Principal parameters for RSA

In order to estimate the various parameters required as input to CRootBox, descriptive statistics and inference are performed on the data gathered from the roots scans. The raw CSV files were processed using the Python programming language and the Spyder software. Nevertheless, all the analyses and plots were conducted using R. The presence of outliers can introduce noise and distorts the true trends in the data. This is achieved through the utilisation of the interquartile range (IQR) method, as previously outlined by Vinutha et al. (2018). The method entails the division of the data sets into four parts, or quartiles. Furthermore, it is stated that the central value of the data set is situated between the third quartile (Q3) and the first quartile (Q1). The IQR is subsequently

calculated as the difference between the upper and lower quartiles. The values exceeding the upper quartile plus one and a half IQR or falling below the lower quartile minus one and a half IQR are excluded. The aforementioned method is then applied to the remaining data set.

To best characterize the architecture of each variety, four parameters were chosen based on important root traits. They were selected because they are the easiest to obtain after tracing the roots in SmartRoot. Additionally, they are included in the inputs for CRootBox. These four parameters are:

1. **Number of root axes,** $maxB$: The number of root axes was counted for each plant. An average was calculated and provided for each variety. This parameter seems crucial because plants with more root axes may exhibit increased root branching and complexity, which can enhance its ability to explore the soil for resources such as water and nutrients. The presence of additional root axes can lead to a more extensive root system that covers a larger volume of soil, potentially improving the plant's capacity to acquire essential resources. Furthermore, a plant with more root axes may have a greater capacity for nutrient uptake and water absorption due to the increased surface area provided by the additional roots. This can contribute to improved plant growth, development, and overall performance, especially under conditions of nutrient limitation or water stress. The enhanced root system architecture resulting from having more root axes can also promote soil stability, erosion control, and ecosystem resilience.

2. **Root radius,** a: was divided into two parts: the radius for the main roots and the radius for the secondary or lateral roots.

3. **Length between lateral branches** l_n: is the inverse of lateral density (1/child-density). This parameter defines the root density in the soil and, consequently, their soil exploration. It corresponds to the average distance between two lateral roots present on the same parent root.

4. **Growth rate** r: is the only parameter that was determined via the rhizotrons experiment, it allows us to observe how well the roots can grow more or less rapidly. This growth rate was calculated for each root, and an average was then taken across all roots for each variety.

CHAPTER 4

RESULTS

In this section is presented the results of the analyses made on the aerial and roots part of the 9 varieties studied. Based on these field results and the collected parameters, simulations with CRootBox will be presented. The RSA will be then used to calculates RSHA with MARSHAL. The Pythons/R scripts made to obtain the graphics and results are accesible on GitHub.

4.1 Aerial part

here, the results for the aerial parts harvested after the experiments will be presented. As explain in the Section 3.2.1, leaves has been dried for 72 hours in order to allow for the measurement of the dry weight of each sample.

4.1.1 Rhizotrons

Dry weight

A type 1 ANOVA analysis was initially conducted for each species. The dependent variable is dry weight, while variety is the independent variable. The objective is to ascertain whether there are any discernible differences between the varieties within each species. The results of these analyses demonstrate that the impact of variety on the species average for dry weight is not statistically significant (at the 5% level of significance) for each species. The results are presented in Table 4.1. Nevertheless, despite the absence of statistically significant differences within a given species, the dotplot (see Figure 4.1) illustrates that there are discernible variations between the species. It is notable that oat exhibit markedly higher dry weight values than the other species. Conversely, spelt and rye appear to be equivalent.

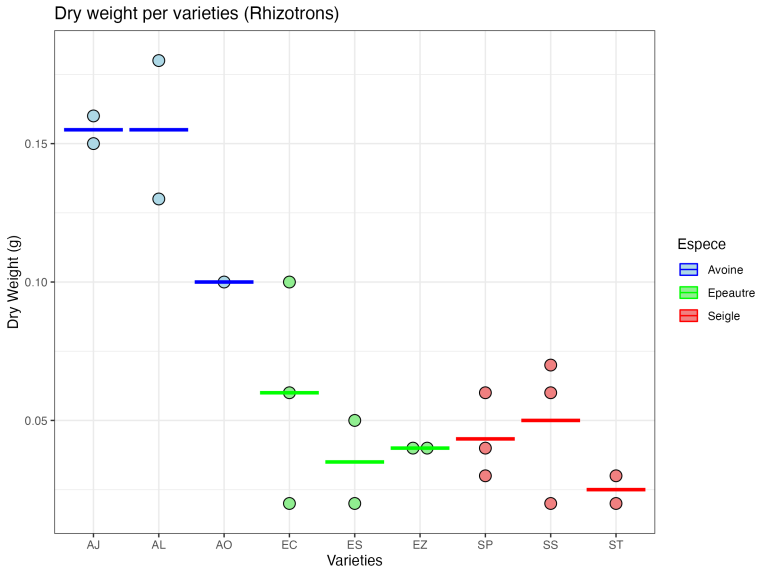

Figure 4.1: Dotplot of the dry weight in the rhizotron experiment for each varieties

ANOVA Oat	**Df**	**Sum Sq**	**Mean Sq**	**F value**	**Pr(>F)**
Varieties	2	0.00242	0.00121	1.862	0.349
Residuals	2	0.00130	0.00065		

(a)

ANOVA Rye	**Df**	**Sum Sq**	**Mean Sq**	**F value**	**Pr(>F)**
Varieties	2	0.0007708	0.0003854	1.005	0.43
Residuals	5	0.0019167	0.0003833		

(b)

ANOVA Spelt	**Df**	**Sum Sq**	**Mean Sq**	**F value**	**Pr(>F)**
Varieties	2	0.000893	0.0004464	0.489	0.646
Residuals	4	0.003650	0.0009125		

(c)

Table 4.1: ANOVA tables for the variety effect on the dry weight for Oat (a), Rye(b), and Spelt(c) respectively in the rhizotron experiment

A type 1 ANOVA was therefore conducted, with the explained variable remaining dry weight, but the explanatory variable being the species to which the plant belongs. This ANOVA corroborated the visual observations on the graphs. The p-value associated with the F-value is well below 0.05, indicating that the effect of the species is statistically significant. The results of this ANOVA are presented in Table 4.2.

To ascertain the distinctions between the species, a Tukey 2 to 2 comparison test was

	Df	Sum Sq	Mean Sq	F value	Pr(>F)
Species	2	0.03763	0.018815	29.21	3.16e-06 ***
Residuals	17	0.01095	0.000644		

Table 4.2: ANOVA table for the species effect on the dry weight in the rhizotron experiment

subsequently conducted. The results of this test also confirm that oat are indeed different from the other two species, but that spelt and rye are not significantly different. The results of this comparison are presented in Table 4.3.

Comparison	Estimate	Std. Error	t value	Pr(> |t|)
Spelt - Oat = 0	-0.096857	0.014861	-6.518	$< 1e-04$ ***
Rye - Oat = 0	-0.102750	0.014469	-7.102	$< 1e-04$ ***
Rye - Spelt = 0	-0.005893	0.013135	-0.449	0.895

Table 4.3: Tukey test between species for the dry weight in the rhizotron experiment

4.1.2 Columns

Development stages

To begin analysing the results, here is the development stage record for each plant studied in the table 4.4. Unfortunately, the seeds in 3 columns did not germinate (AJ2, AL3 and SP1) and it was therefore impossible to take notes for them.

Varieties	BBCH Scale
AJ1	22
AJ3	21
SS1	24
SS2	23
SS3	24
EC1	24
EC2	23
EC3	23
AO1	22
AO2	21
AO3	21
AL2	22

Varieties	BBCH Scale
ST1	26
ST2	25
ST3	24
ES1	23
ES2	23
ES3	22
AL1	23
SP2	21
SP3	23
EZ1	23
EZ2	23
EZ3	24

Table 4.4: Aerial part results (BBCH scale)

From the observations made in the Table 4.4, all plants have reached the second stage of development, corresponding to tillering. Therefore, it is not possible to discern differ-

ences among them at this stage. However, they differ in the number of leaves indicated by the second digit of the BBCH number. Apart from the variety Seigle Poséidon (SP), which appears to have, on average, a more advanced developmental stage compared to the other varieties, the rest of the varieties seem to be equivalent regarding this variable.

Dry weight

As with the rhizotrons, a type 1 ANOVA was carried out for each species to see if there were differences within varieties. This ANOVA showed that the effect of variety on the species mean was not significant for $\alpha < 0.05$. The results of these ANOVAs are shown in table 4.5.

ANOVA Oat	**Df**	**Sum Sq**	**Mean Sq**	**F value**	**Pr(>F)**
Varieties	2	0.02728	0.01364	0.414	0.686
Residuals	4	0.13172	0.03293		

(a)

ANOVA Rye	**Df**	**Sum Sq**	**Mean Sq**	**F value**	**Pr(>F)**
Varieties	2	0.07662	0.03831	1.321	0.346
Residuals	5	0.14498	0.02900		

(b)

ANOVA Spelt	**Df**	**Sum Sq**	**Mean Sq**	**F value**	**Pr(>F)**
Varieties	2	0.1756	0.08781	3.033	0.123
Residuals	6	0.1737	0.02896		

(c)

Table 4.5: ANOVA table for the variety effect on the dry weight for Oat (a), Rye(b) and Spelt(c) in the column experiment

Upon examination of Figures 4.2, it becomes evident that discerning a distinct and discernible divergence between the species is challenging, with the exception of rye, which exhibits elevated dry weight values.

An ANOVA 1 was then carried out with species as the explanatory factor for dry weight. We can see that the species effect is significant for $\alpha < 0.05$. The results of the ANOVA are shown in Table 4.6. A Tukey test was performed to determine the differences between the species. It shows that rye differs from the other 2 species. Furthermore, the difference between rye and spelt is much more significant than that between rye and oat. The results of this test are given in Table 4.7.

In conjunction with this section on aerial parts in the column experiment, it can be

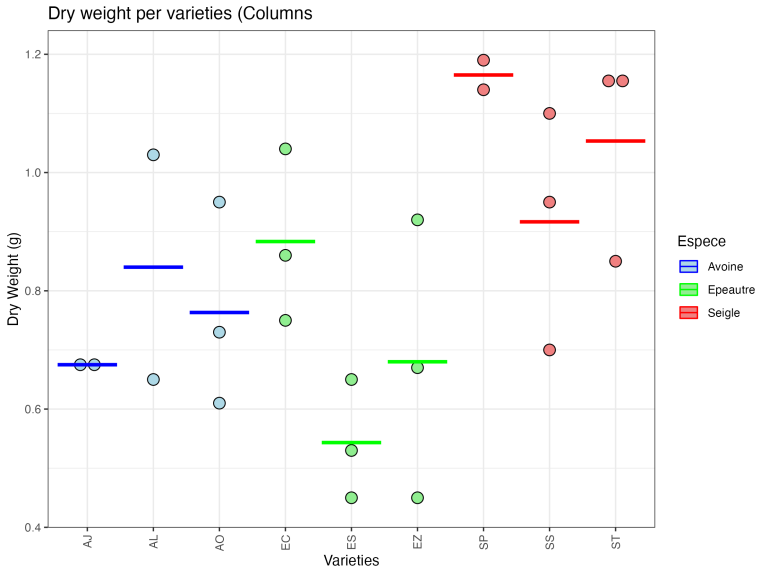

Figure 4.2: Dotplot of the dry weight in the column experiment for each varieties

	Df	Sum Sq	Mean Sq	F value	Pr(>F)
Species	2	0.5012	0.25059	7.209	0.00413 **
Residuals	21	0.7300	0.03476		

Table 4.6: ANOVA table for the species effect on the dry weight in the column experiment

Comparison	Estimate	Std. Error	t value	Pr(> $\|t\|$)
Spelt - Oat = 0	-0.05778	0.09396	-0.615	0.81350
Rye - Oat = 0	0.27000	0.09649	2.798	0.02796 *
Rye - Spelt = 0	0.32778	0.09059	3.618	0.00435 **

Table 4.7: Tukey test between species for the dry weight in the column experiment

observed that all the plants are in phase in their aerial development, with the exception of one variety of rye which appears to be ahead of the others. When dry weight is considered, rye differs from the other two species in having a higher dry weight. It may be hypothesised that the presence of a variety with a higher stage of development influences this dry weight, due to the fact that more leaves also mean more carbon and therefore more dry weight.

4.2 Roots part

This section presents the results pertaining to the root systems of the sampled plants. Each parameter is discussed in the context of the dataset presented in Section 3.5. The majority of the parameters were derived from the column experiment, while the growth rate was measured using rhizotrons.

4.2.1 Number of root axes $maxB$

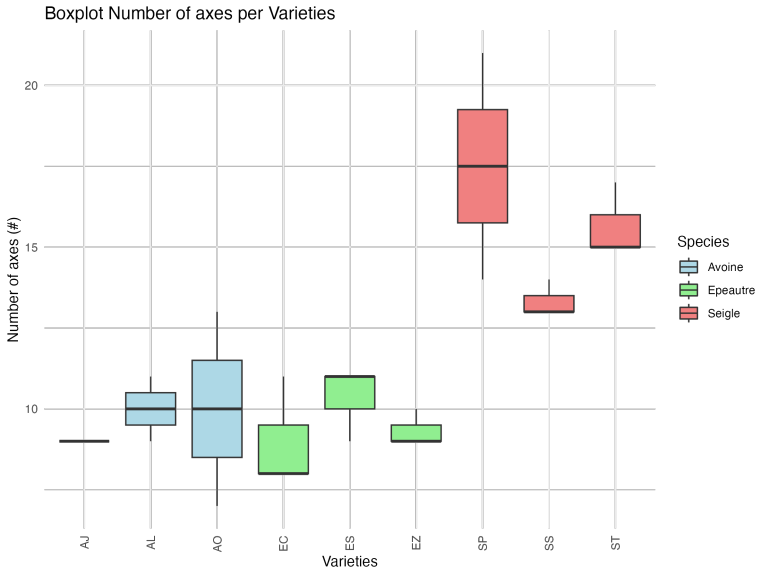

Figure 4.3: Boxplot of the number of axes per varieties

In order to identify and compare the different species, we can begin by examining the number of root axes that each of the varieties studied in this study can produce. The boxplot 4.3 reveals that rye exhibits a distinctive profile, diverging from the other two species, spelt and oat, which display a more similar pattern.

Table 4.8 shows that variety has no significant effect on the species mean. We can run an ANOVA to see if there are any significant differences between the species. The results can be found in Table 4.9. We can see that the species effect is significant. We now need to see which species differ from each other. A Tukey test is then performed and is available in the Table 4.10. This test shows that rye is significantly different from oat and spelt. It confirms the visual impressions in the Boxplot 4.3.

Ultimately, the data in Table 4.10, which collates the mean values, standard deviations and standard errors for each species, will be employed in the simulations that will be conducted subsequently.

ANOVA Oat	**Df**	**Sum Sq**	**Mean Sq**	**F value**	**Pr(>F)**
Varieties	2	1.429	0.714	0.143	0.871
Residuals	4	20.000	5.000		

(a)

ANOVA Rye	**Df**	**Sum Sq**	**Mean Sq**	**F value**	**Pr(>F)**
Varieties	2	21.67	10.833	1.946	0.237
Residuals	5	27.83	5.567		

(b)

ANOVA Spelt	**Df**	**Sum Sq**	**Mean Sq**	**F value**	**Pr(>F)**
Varieties	2	2.889	1.444	0.929	0.445
Residuals	6	9.333	1.556		

(c)

Table 4.8: ANOVA table for the variety effect on the number root axes for Oat (a), Rye(b) and Spelt(c)

	Df	**Sum Sq**	**Mean Sq**	**F value**	**Pr(>F)**
Species	2	168.85	84.42	21.32	8.79e-06 ***
Residuals	21	83.15	3.96		

Table 4.9: ANOVA table for the species effect on the root number axes

Comparison	**Estimate**	**Std. Error**	**t value**	**Pr(> $\|t\|$)**
Spelt - Oat = 0	-0.1587	1.0028	-0.158	0.986278
Rye - Oat = 0	5.5357	1.0299	5.375	0.000111 ***
Rye - Spelt = 0	5.6944	0.9669	5.889	< 1e-04 ***

Table 4.10: Tukey test between Species on the root number axes

Species	**Mean**	**Standard Deviation**	**Standard Error**
Oat	9.714286	1.889822	0.7142857
Rye	15.250000	2.659216	0.9401748
Spelt	9.555556	1.236033	0.4120110

Table 4.11: General means, standard deviation and standard error for the number of root axes for each species

4.2.2 Growth rate r

The growth rate of the roots was quantified through point measurements taken on the rhizotrons. The results of the boxplot distributions are illustrated in Figure 4.4. It can be observed that no variety or species exhibits a distinctive growth pattern. This will be corroborated by the ANOVA 1 test, which has been conducted to ascertain the impact of the species in question. The results of this ANOVA are presented in Table 4.12 and demonstrate that none of the effects are statistically significant in terms of their impact on the element in comparison to the overall mean. Given this result, we can skip the Tukey comparison test.

	Df	**Sum Sq**	**Mean Sq**	**F value**	**Pr(>F)**
Species	2	2.0	0.9855	0.69	0.502
Residuals	242	345.4	1.4273		

Table 4.12: ANOVA table for the species effect on the growth rate

An additional analysis of variance (ANOVA) was conducted to assess the significance of the variety effect on each species. The results (see Table 4.13) indicate that the variety has no impact, despite the p-value for rye being very close to the value $\alpha = 0.05$.

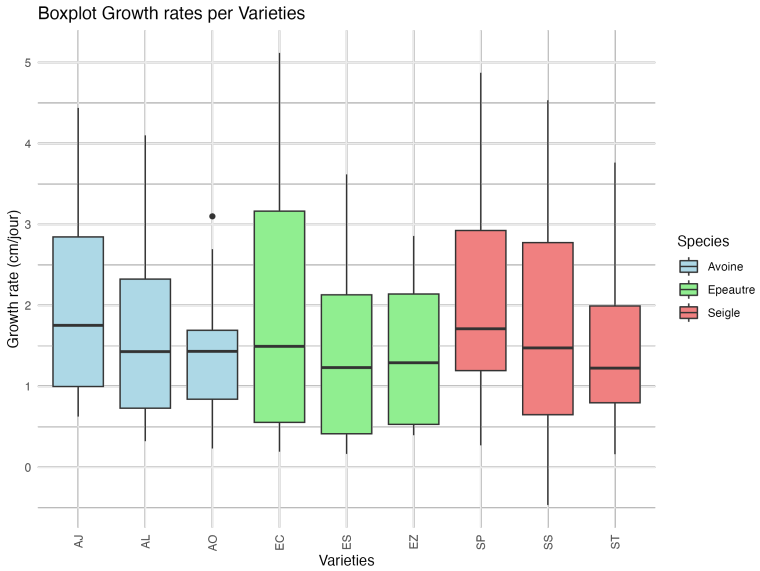

Figure 4.4: Box plot growth rates (cm/day)

The data in the Table 4.14, which collates the mean values, standard deviations and standard errors for each species, will be employed in the simulations that will be conducted subsequently.

ANOVA Oat	**Df**	**Sum Sq**	**Mean Sq**	**F value**	**Pr(>F)**
Varieties	2	3.53	1.766	1.522	0.226
Residuals	62	71.92	1.160		

(a)

ANOVA Rye	**Df**	**Sum Sq**	**Mean Sq**	**F value**	**Pr(>F)**
Varieties	2	7.97	3.984	2.815	0.0642
Residuals	111	157.07	1.415		

(b)

ANOVA Spelt	**Df**	**Sum Sq**	**Mean Sq**	**F value**	**Pr(>F)**
Varieties	2	2.14	1.072	0.657	0.522
Residuals	63	102.77	1.631		

(c)

Table 4.13: ANOVA table for the variety effect for the growth rate for Oat (a), Rye(b) and Spelt(c)

Species	**Mean**	**Standard Deviation**	**Standard Error**
Oat	1.733450	1.085809	0.1346780
Rye	1.848101	1.208504	0.1131868
Spelt	1.634450	1.270481	0.1563854

Table 4.14: General means, standard deviation and standard error for the growth rate for each species

4.2.3 Roots diameter $2 * a$

This section will distinguish between the diameter of primary roots (also known as nodal roots) and the diameter of associated lateral roots. The CRootBox system is capable of providing inputs for each root type. Subsequently, these diameters will be divided by two in order to obtain the requisite radii for CRootBox. (see Table 3.3)

Diameter of the main roots

As illustrated in the boxplot (see Figure 4.5), the EC variety exhibits the smallest diameter, which is evident as a notable outlier. Nevertheless, the data indicates that the other species exhibit a similar diameter range. A preliminary set of one-way analysis of variance (ANOVA) tests was conducted on each variety within each species. The results of this test, as presented in Table 4.15, indicate that the effect of variety has a significant impact on the overall average for rye and spelt. Subsequently, a Tukey test may be employed for the purpose of comparing the varieties in pairs. The results of the

Tukey test (see Table 4.16 and Table 4.17) indicate that there are significant differences between the EC varieties and the rest of the spelt varieties and the SS and SP varieties, with a significance level of $\alpha = 0.05$. The discrepancy between the ST and SP groups is statistically significant, yet insufficient to substantiate our hypothesis.

ANOVA Oat	**Df**	**Sum Sq**	**Mean Sq**	**F value**	**Pr(>F)**
Varieties	2	0.0187	0.009366	0.758	0.473
Residuals	63	0.7787	0.012361		

(a)

ANOVA Rye	**Df**	**Sum Sq**	**Mean Sq**	**F value**	**Pr(>F)**
Varieties	2	0.0641	0.03207	3.648	0.029 *
Residuals	119	1.0462	0.00879		

(b)

ANOVA Spelt	**Df**	**Sum Sq**	**Mean Sq**	**F value**	**Pr(>F)**
Varieties	2	0.3512	0.17559	22.11	9.21e-09 ***
Residuals	107	0.8499	0.00794		

(c)

Table 4.15: ANOVA table for the variety effect for the diameter of the main root for Oat (a), Rye(b) and Spelt(c)

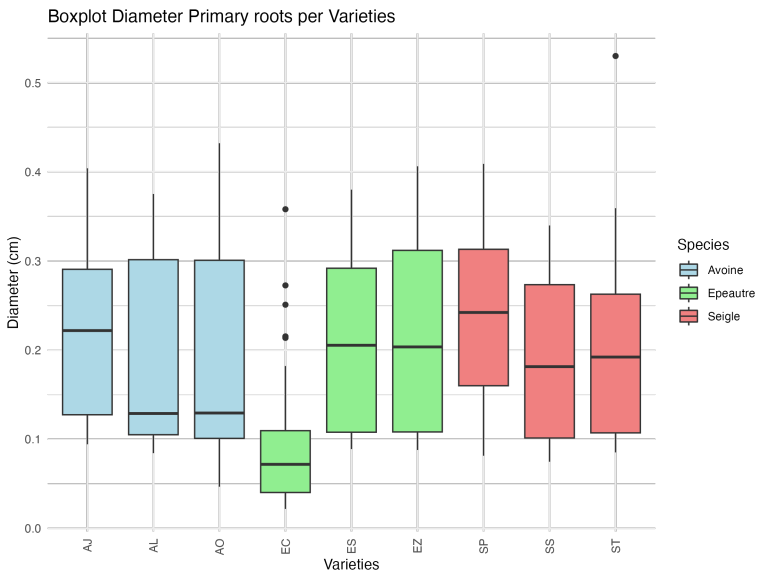

Figure 4.5: Box plot main diameter (cm)

Comparison	Estimate	Std. Error	t value	Pr(> |t|)
SS - SP = 0	-0.053855	0.021702	-2.482	0.0382 *
ST - SP = 0	-0.047330	0.020934	-2.261	0.0654 .
ST - SS = 0	0.006526	0.020170	0.324	0.9439

Table 4.16: Tukey test between varieties of rye on the main root diameter

Comparison	Estimate	Std. Error	t value	Pr(> |t|)
ES - EC = 0	0.110721	0.020374	5.435	<1e-05 ***
EZ - EC = 0	0.116263	0.020803	5.589	<1e-05 ***
EZ - ES = 0	0.005543	0.023024	0.241	0.968

Table 4.17: Tukey test between Varieties of spelt on the main root diameter

Once the ANOVAs have been conducted on the varieties, a comparison between the species can be undertaken. A type 1 ANOVA was then conducted, which revealed a statistically significant difference between the species (see Table 4.18). The Tukey comparison test, as illustrated in Table 4.19, indicates that spelt exhibits a statistically significant difference from the other two species, as evidenced by the boxplot. It is plausible that this discrepancy is attributable to the fact that the EC variety possesses a notably smaller diameter in comparison to the other samples.

	Df	Sum Sq	Mean Sq	F value	Pr(>F)
Species	2	0.1873	0.09363	8.885	0.000179 ***
Residuals	295	3.1088	0.01054		

Table 4.18: ANOVA table for the species effect on the main root diameter

Comparison	Estimate	Std. Error	t value	Pr(> |t|)
Spelt - Oat = 0	-0.04420	0.01598	-2.766	0.016469 *
Rye - Oat = 0	0.01085	0.01569	0.692	0.767716
Rye - Spelt = 0	0.05505	0.01350	4.079	0.000166 ***

Table 4.19: Tukey test between Species on the main root diameter

The data in the Table 4.20, which collates the mean values, standard deviations and standard errors for each species for the main root diameter, will be employed in the simulations that will be conducted subsequently.

Groupe	Mean	Standard Deviation	Standard Error
Oat	0.1967697	0.11076304	0.013633988
Rye	0.2076180	0.09579158	0.008672562
Spelt	0.1525668	0.10497116	0.010008608

Table 4.20: General means, standard deviation and standard error for each species for main root diameter

Diameter of the Lateral roots

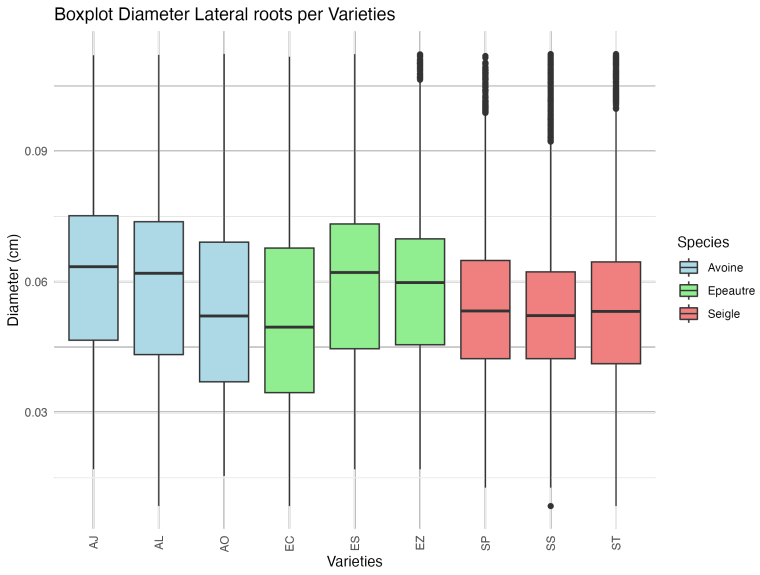

Figure 4.6: Box plot diameter lateral roots

Once the diameters of the main roots have been established, the subsequent step is to ascertain the diameters of the lateral roots. It is evident that these diameters are smaller than those of the main roots. It should be noted that this parameter will not be utilized in the CRootBox model; rather, the radius will be employed. To conclude, the boxplot analysis for this parameter (see Figure 4.6) reveals that all varieties and species exhibit a similar distribution of values. No particular variety or species stands out. Therefore, it is necessary to examine the ANOVA 1s for all varieties within each species to ascertain whether any significant differences exist.

As evidenced by the results of the ANOVA, there is a significant diversity of mean diameters within each species (see Table 4.21, Table 4.22, and Table 4.23). A Tukey test was conducted for each species (it should be noted that this is the first occasion on which the ANOVA has yielded significant results for each species). The results demonstrated that:

- For oat, as illustrated in Table 4.24, all varieties exhibit notable differences from one another, with the AO variety displaying the most pronounced divergence from

	Df	Sum Sq	Mean Sq	F value	Pr(>F)
Varieties	2	0.128	0.06415	151.9	<2e-16 ***
Residuals	11854	5.007	0.00042		

Table 4.21: ANOVA table for the variety effect of the diameter of the laterals root for oat

	Df	Sum Sq	Mean Sq	F value	Pr(>F)
Varieties	2	0.005	0.0024196	8.638	0.000178 ***
Residuals	25536	7.153	0.0002801		

Table 4.22: ANOVA table for the variety effect of the diameter of the lateral root for rye

	Df	Sum Sq	Mean Sq	F value	Pr(>F)
Varieties	2	0.204	0.10184	279.1	<2e-16 ***
Residuals	17087	6.235	0.00036		

Table 4.23: ANOVA table for the variety effect of the diameter of the lateral root for spelt

the other two with the lowest diameter. AJ is greater than AL.

- For rye, as illustrated in Table 4.25, the SS variety exhibits a smaller mean than the other two. The p-values for the ST and SP varieties are greater than 0.05, indicating that their difference is not statistically significant.

- For spelt as illustrated in Table 4.26, it is evident that variety EC exhibits an inferior mean in comparison to varieties ES and EZ, as evidenced by the elevated p-values associated with its tests. With regard to the remaining two varieties, it can be observed that ES exhibits a higher mean than that of EZ.

Comparison	Estimate	Std. Error	t value	Pr(> $\|t\|$)
AL - AJ == 0	-0.0017692	0.0005044	-3.507	0.00129 **
AO - AJ == 0	-0.0075243	0.0004783	-15.730	< 1e-04 ***
AO - AL == 0	-0.0057551	0.0004383	-13.132	< 1e-04 ***

Table 4.24: Tukey test between varieties of oat on the lateral roots diameter

Comparison	Estimate	Std. Error	t value	Pr(> |t|)
SS - SP = 0	-0.0010910	0.0002716	-4.016	0.000169 ***
ST - SP = 0	-0.0004368	0.0002731	-1.599	0.245160
ST - SS = 0	0.0006542	0.0002407	2.718	0.017988 *

Table 4.25: Tukey test between varieties of rye on the lateral roots diameter

Comparison	Estimate	Std. Error	t value	Pr(> |t|)
ES - EC = 0	0.0082615	0.0003701	22.32	< 1e-05 ***
EZ - EC = 0	0.0066412	0.0003582	18.54	< 1e-05 ***
EZ - ES = 0	-0.0016203	0.0003499	-4.63	1.07e-05 ***

Table 4.26: Tukey test between varieties of spelt on the lateral roots diameter

Now that the analysis of the varieties has been completed, we can proceed to the comparison of the species. To this end, an ANOVA 1 was conducted (see Table 4.27), which revealed a statistically significant species effect and a mean difference in lateral root diameter between species.

	Df	Sum Sq	Mean Sq	F value	Pr(>F)
Species	2	0.192	0.09616	279.7	<2e-16 ***
Residuals	54483	18.732	0.00034		

Table 4.27: ANOVA table for the species effect on the lateral roots diameter

As illustrated in Figure 4.28, the Tukey test reveals significant inter-species differences. The highest average was observed in oat, followed by spelt and then rye.

Comparison	Estimate	Std. Error	t value	Pr(> |t|)
Spelt - Oat = 0	-0.0012831	0.0002216	-5.79	1.73e-08 ***
Rye - Oat = 0	-0.0044079	0.0002061	-21.39	< 1e-08 ***
Rye - Spelt = 0	-0.0031248	0.0001833	-17.05	< 1e-08 ***

Table 4.28: Tukey test between species on the lateral roots diameter

Ultimately, the numerical values utilized in the CRootBox model are presented in Table 4.29, which corroborates the findings of the Tukey test.

Groupe	Mean	Standard Deviation	Standard Error
Oat	0.05856772	0.02081176	0.0001911267
Rye	0.05415985	0.01674207	0.0001047628
Spelt	0.05728463	0.01941094	0.0001484826

Table 4.29: General means, standard deviation and standard error for each species for lateral roots diaemeter

4.2.4 Inter lateral distance

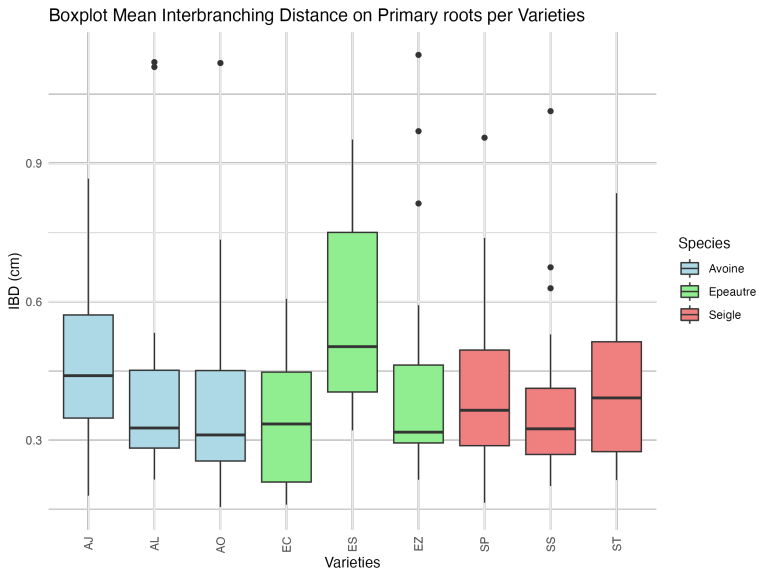

Figure 4.7: Boxplot of the IBD of the main roots per varieties

We may now proceed to the final variable of interest, namely the mean distance between laterals. As previously stated, this is the inverse of the density of laterals on a main root. As illustrated in Figure 4.7, the Boxplot reveals that specific varieties, including AJ, ES, and SS, exhibit distinctive characteristics compared to other varieties within the same category. The objective is to ascertain whether the variety effect is significant by conducting an ANOVA 1 between each species. Despite the visual observations, there is no statistical evidence to suggest that there is a difference between varieties for oat and rye (see Subtables (a) and (b) of Table 4.30). Nevertheless, a statistical difference is observed for spelt (see Subtables (c) of the Table 4.30).

To ascertain the specific varieties that differentiate within the spelt species, a Tukey test was conducted (see Table 4.31). This demonstrates that the ES and EC varieties are distinct from one another. The variety EC exhibited the lowest IBD, while the variety ES demonstrated the highest.

ANOVA Oat	**Df**	**Sum Sq**	**Mean Sq**	**F value**	**Pr(>F)**
Varieties	2	0.0604	0.03018	0.547	0.582
Residuals	50	2.7578	0.05516		

(a)

ANOVA Rye	**Df**	**Sum Sq**	**Mean Sq**	**F value**	**Pr(>F)**
Varieties	2	0.0588	0.02942	0.855	0.429
Residuals	80	2.7535	0.03442		

(b)

ANOVA Spelt	**Df**	**Sum Sq**	**Mean Sq**	**F value**	**Pr(>F)**
Varieties	2	0.515	0.25749	5.916	0.00475 **
Residuals	54	2.350	0.04352		

(c)

Table 4.30: ANOVA table for the variety effect on the IBD for Oat (a), Rye(b) and Spelt(c)

Comparison	**Estimate**	**Std. Error**	**t value**	**Pr(> $\|t\|$)**
ES - EC = 0	0.23392	0.06806	3.437	0.0032 **
EZ - EC = 0	0.09621	0.06605	1.457	0.3196
EZ - ES = 0	-0.13771	0.06965	-1.977	0.1275

Table 4.31: Tukey test between varieties of spelt on the IBD

Now that the distinction between varieties of spelt has been established, the possibility of the existence of mean value differences between species is going to be studied. The ANOVA result (see Table 4.32) demonstrates that there are no statistically significant differences between the species. Consequently, a Tukey test is not required.

	Df	**Sum Sq**	**Mean Sq**	**F value**	**Pr(>F)**
Species	2	0.044	0.02224	0.497	0.609
Residuals	190	8.496	0.04471		

Table 4.32: ANOVA table for the species effect on the IBD

Ultimately, the numerical values utilized in the CRootBox model are presented in Table 4.33.

Groupe	Mean	Standard Deviation	Standard Error
Oat	0.4232219	0.2328003	0.03197758
Rye	0.4074109	0.1851949	0.02032778
Spelt	0.4436722	0.2261947	0.02996023

Table 4.33: General means, standard deviation and standard error for each species for IBD

4.2.5 Final parameters table for CRootBox

Table 4.34 illustrates the complete set of parameter values employed as inputs in the CRootBox model. The parameters highlighted in yellow have been estimated using the averages for each species. In CRootBox, the aforementioned parameters are divided into two sections. The first of these is *rparam*, which involves the elements highlighted in blue. This file contains the parameters specific to the roots. The remaining section is the *pparam* file, highlighted in red, which encompasses the parameters exclusive to the plant. The values of the a parameters (for the primary and lateral roots) differ from the data presented in Tables 4.20 and 4.29 due to the fact that they have been divided by two in order to obtain the radius.

The parameters that have already been estimated are those that are present in the CRootBox database. The dataset serves as the parameter file for Triticum aestivum (Schnepf et al., 2018). The data were obtained from the Bingham and Wu (2011) studies, which employed the SPACSYS method to analyse wheat root architecture.

The selection of 40 days of simulation has been made because it marks the conclusion of the plant's vegetative phase and the subsequent reduction in growth. This is due to the onset of vernalisation, a period of cold exposure undergone by a plant to facilitate its transition from the vegetative stage to the reproductive stage, namely, the initiation of flowering. (Bingham and Wu, 2011; Jong Un, 1993).

The *rparam* file contains the requisite parameters for the secondary and tertiary lateral roots. Nevertheless, these factors will not be incorporated into the model. Indeed, during the course of my research, I observed that there were no instances of lateral roots developing on the first order lateral roots. In order to maintain the highest degree of realism, it was decided that these roots should be eliminated. Furthermore, the architectural plot will facilitate a more comprehensive understanding of the primary root development..

Root type	Parameters	WHEAT	OAT	RYE	SPELT
basalroot	l_b	0.8008			
basalroot	l_a	12			
basalroot	l_n	0.25	0.4232219	0.4074109	0.4436722
basalroot	l_{max}	60			
basalroot	r	2.4	1.733450	1.848101	1.634450
basalroot	a	0.05	0.09838487	0.10380900	0.07628341
basalroot	n_tropism	0.5			
basalroot	sigma_tropism	0.261799			
basalroot	tropism	1			
basalroot	dx	5			
basalroot	successors	1			
basalroot	successorP	1			
basalroot	theta	0.78			
basalroot	rlt	1000000000			
basalroot	gf	1			
1storderlateral	l_b	1			
1storderlateral	l_a	5			
1storderlateral	l_n	0.25			
1storderlateral	l_{max}	10			
1storderlateral	r	0.6			
1storderlateral	a	0.03	0.02928386	0.02707993	0.02864231
1storderlateral	n_tropism	1			
1storderlateral	sigma_tropism	0.5			
1storderlateral	tropism	1			
1storderlateral	dx	5			
1storderlateral	successors	1			
1storderlateral	successorP	1			
1storderlateral	theta	0.785398			
1storderlateral	rlt	1000000000			
1storderlateral	gf	1			
plant	plantingdepth	3			
plant	firstB	0			
plant	delayB	0			
plant	maxB	16	9.714286	15.250000	9.555556
plant	nC	0			
plant	firstSB	1000			
plant	delaySB	1000			
plant	delayRC	1000			
plant	nz	0			
plant	simtime	40			

Table 4.34: Final parameters table for CRootBox

4.3 RSA simulation with CrootBox

In this section is presented all the simulations made with CRootBox for each species.

4.3.1 Rye

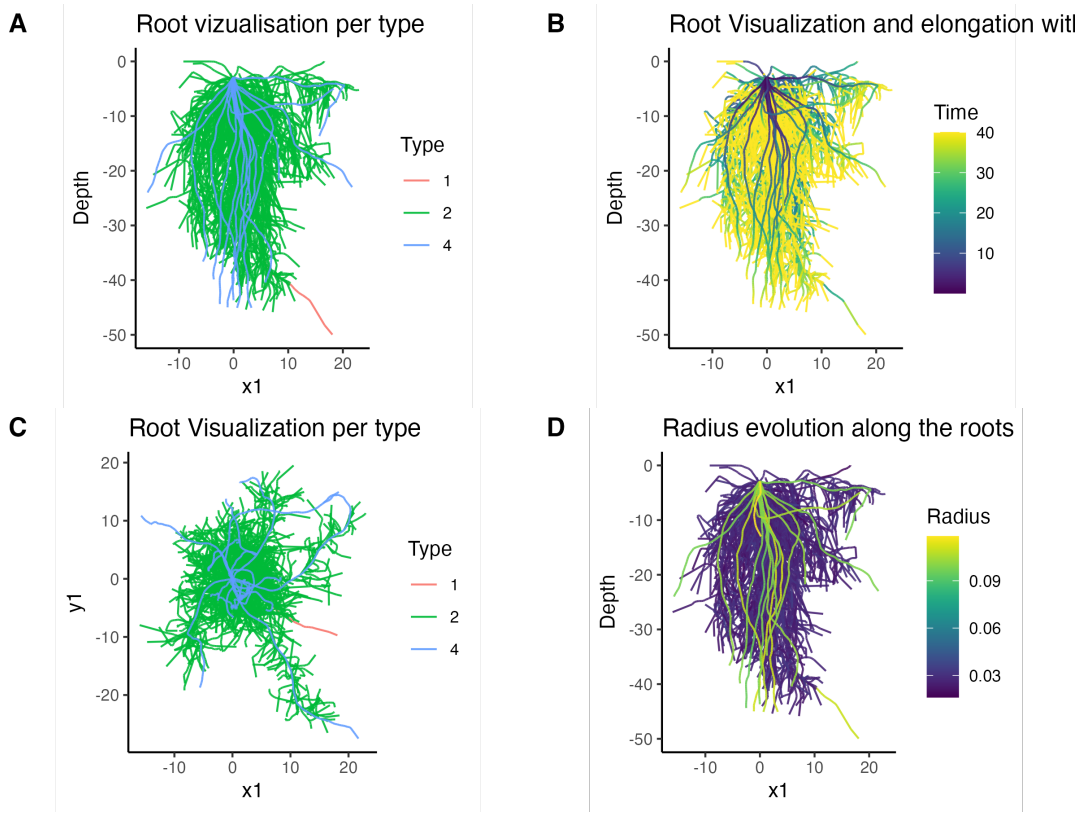

Figure 4.8: Root Visualization for rye after 40 days

The results of the simulations conducted with the collected parameters for rye after 40 days of growth are presented herewith (see Figure 4.8). The graph in **Graph A** illustrates the various root types that were modeled. **Graph B** depicts the temporal evolution of each root and their emergence. The greater the clarity, the older the root. **Graph C** depicts the same element as Graph **Graph A**, but from an overhead perspective. **Graph D** illustrates the evolution of root radius along the architectural structure.

As previously stated, only adventitious roots and first-order lateral roots are depicted. The root system is composed of large-radius adventitious roots. These penetrate deeply into the soil, giving rise to lateral roots that are smaller in radius and more constant, thereby enabling the soil to be explored more thoroughly. Additionally, the temporal evolution of the roots illustrates the initial formation of the main roots, which continue to grow until day 30. Additionally, the lateral roots are predominantly situated at the outset of the main roots, which aligns with the earlier proposition that lateral roots are only generated when the basal and apical zones are fully mature. This elucidates the rationale behind the time required for a lateral root to emerge.

Figure 4.9 illustrates the simulation of the evolution of a rye root system with a 5 days period between the observations. We can see that within the initial five-day period, the

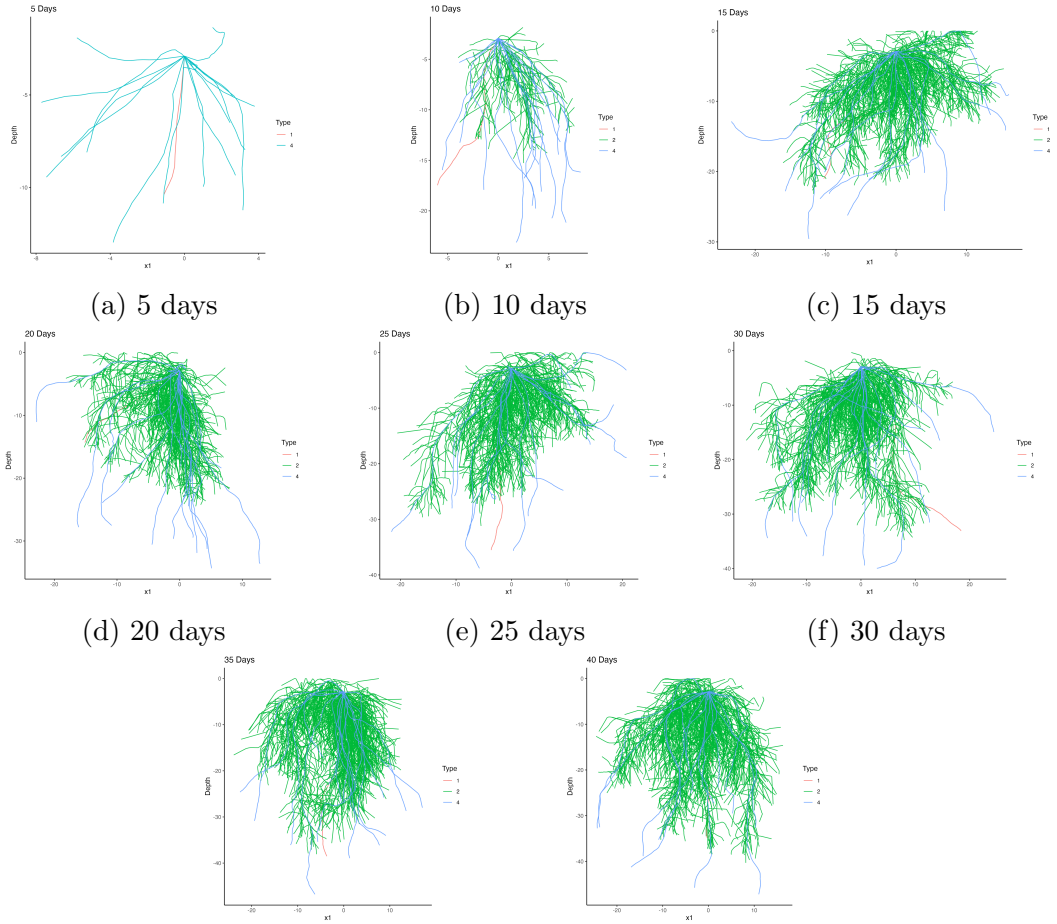

(a) 5 days (b) 10 days (c) 15 days

(d) 20 days (e) 25 days (f) 30 days

(g) 35 days (h) 40 days

Figure 4.9: Root visualization at 5 days interval for rye

vast majority of the main roots have emerged and are undergoing rapid growth. However, the formation of lateral roots has not yet begun. The emergence of lateral roots will begin in the subsequent days. With regard to the remaining observations, it is difficult to offer any definitive conclusions other than that the density of lateral roots is increasing and that the primary roots are following their typical trajectory. Nevertheless, it can be demonstrated that this cessation of growth may be attributed to the maximum length parameter (l_{max}), which has been set at 60 cm and thus prevents the root system from extending beyond this point.

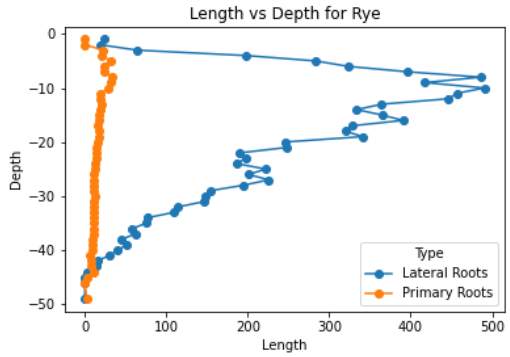

(a) Total Root length in fuction of depth for Rye

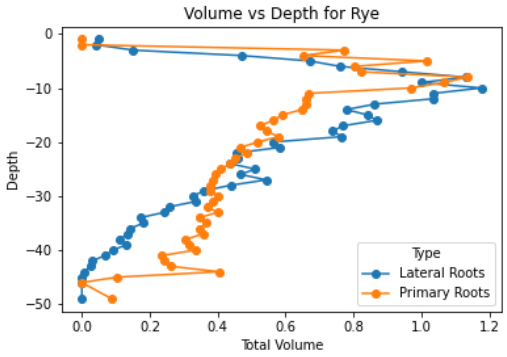

(b) Total Volume of roots in function of depth for Rye

Figure 4.10: Underground representation of the rye root system

Figure 4.10a shows the evolution of root length by type. Most of the contribution to this total lengths comes from the lateral roots. This makes sense because the main roots number are 10 on average, whereas lateral roots number can be thousands. What is also noticeable is the rather uniform distribution of root length for the main roots in terms of depth, showing that the roots grow towards the bottom and do not go to the side. This is in contrast to the lateral roots, which, as we explained earlier, are located at the start of the main roots, explaining the strong localisation of root lengths close to the surface. In the end, there are few lateral roots in the deeper parts.

However, the fact that root length is primarily influenced by lateral roots does not necessarily imply that this is also the case for the distribution of volume. Indeed, an examination of Figure 4.10b reveals that it is the main roots that exert a greater influence over the lateral roots. This can be attributed to the fact that their radius is approximately three times greater. Table 4.35 corroborates the assertion that primary roots possess the greatest root volume but the shortest total root length.

Type	**Volume** (cm^3)	**Length(cm)**
Lateral Roots	21.161516	9102.5755
Primary Roots	22.251918	663.3211

Table 4.35: Sum of the volumes and length per root type for rye

4.3.2 Oat

The results of the simulations conducted with the collected parameters for oat after 40 days of growth are presented in Figure 4.11. The same observations presented in Section 4.3.1 are reiterated herewith. Additionally, Graph **B** illustrates that the temporal evolution of the roots demonstrates that the formation of the main roots occurs first, followed by the formation of laterals, which continue to grow until day 40. The radius of the main roots exhibits considerable variation, whereas that of the lateral roots is relatively constant.

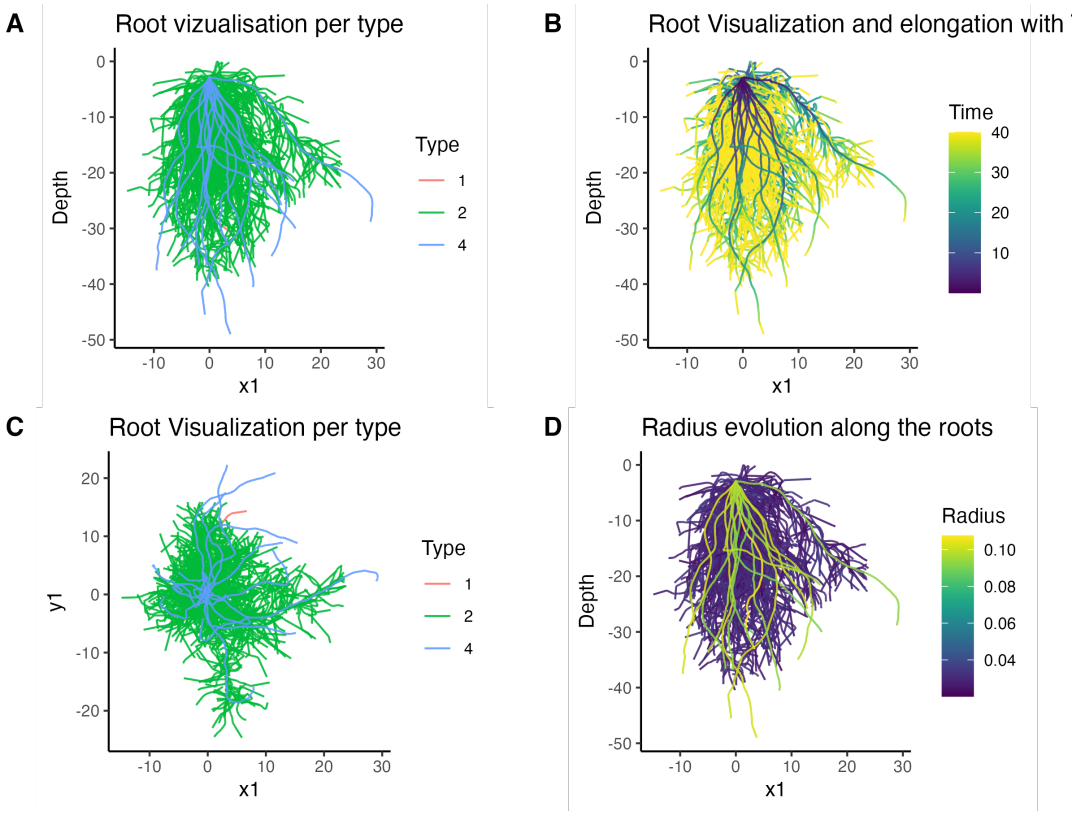

Figure 4.11: Root visualization for oat after 40 days

Figure 4.12 illustrates the simulation of the evolution of a oat root system with a five-day period between observations. As previously stated with regard to rye, all of the main roots are formed within a five-day period following seeding. The emergence of the first laterals is observed on day 10, reaching their maximum length with minimal subsequent growth. The emergence of lateral roots persists for as long as the main root continues to grow, until it attains its maximal length.

Figure 4.13a shows the evolution of root length by type. Just like for rye, most of the contribution to this total length comes from the lateral roots. Lateral roots tend to grow in the upper part of the soil and primary roots are uniformly scatter along the depth.

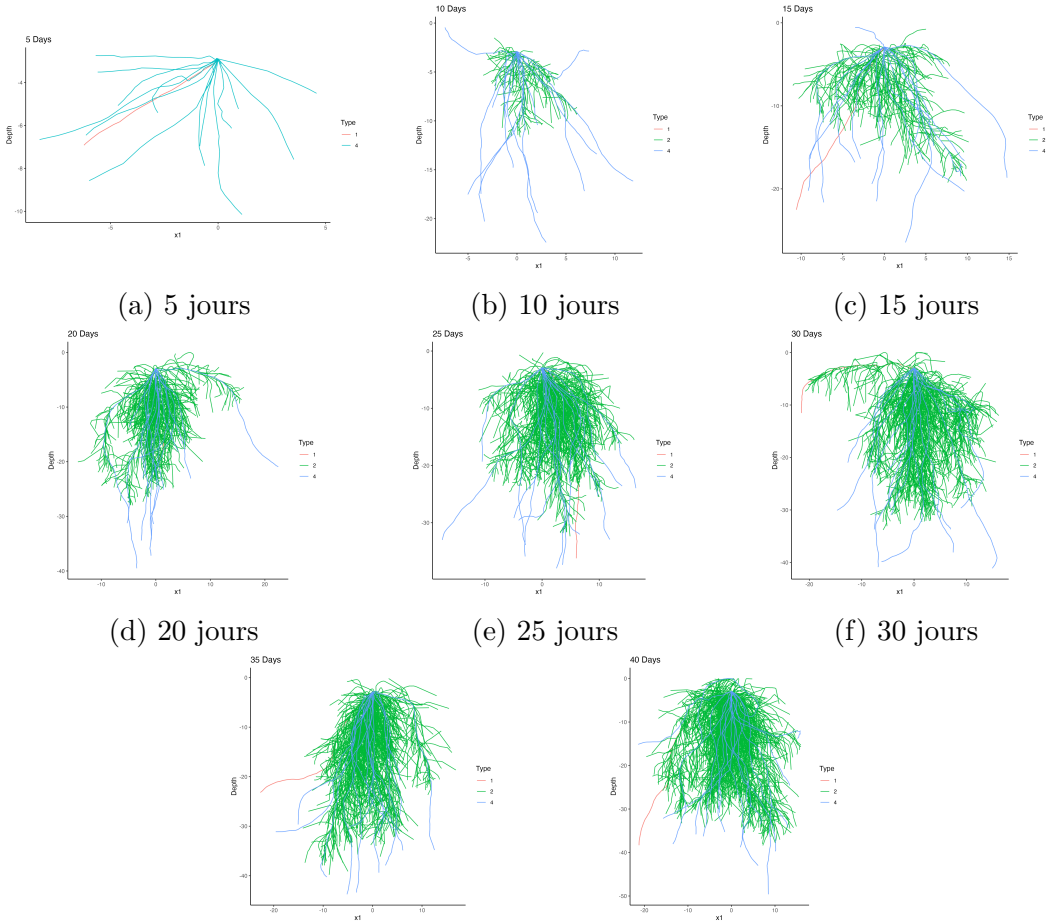

(a) 5 jours (b) 10 jours (c) 15 jours

(d) 20 jours (e) 25 jours (f) 30 jours

(g) 35 jours (h) 40 jours

Figure 4.12: Root visualization at 5 days interval for oat

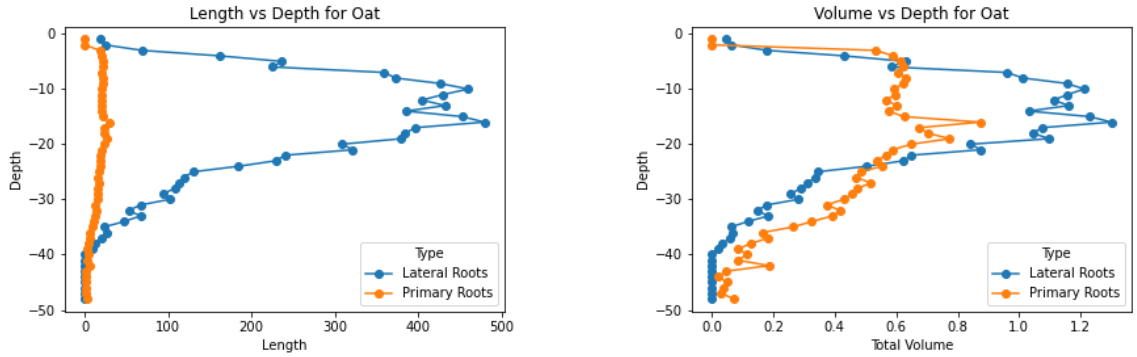

(a) Total Root length in fuction of depth for Oat

(b) Total Volume of roots in function of depth for Oat

Figure 4.13: Underground representation of the oat root system

Figure 4.10b shows that most of the roots volume is attributed to the lateral roots. It is then different than rye. This can be attributed to the fact that the radius of oat is smaller than the radius of rye. Table 4.36 corroborates the assertion that lateral roots possess the greatest root volume and the longest total root length.

Type	Volume (cm^3)	Length(cm)
Lateral Roots	22.660705	8369.3774
Primary Roots	19.500089	661.1079

Table 4.36: Sum of the volumes and lengths per root type for oat

4.3.3 Spelt

The results of the simulations conducted with the collected parameters for spelt after 40 days of growth are presented in the following Figure 4.11. The same observations presented in Section 4.3.1 and 4.3.2 are reiterated herewith. No additional observations can be made, except to note that the main roots are slightly more distant from one another.

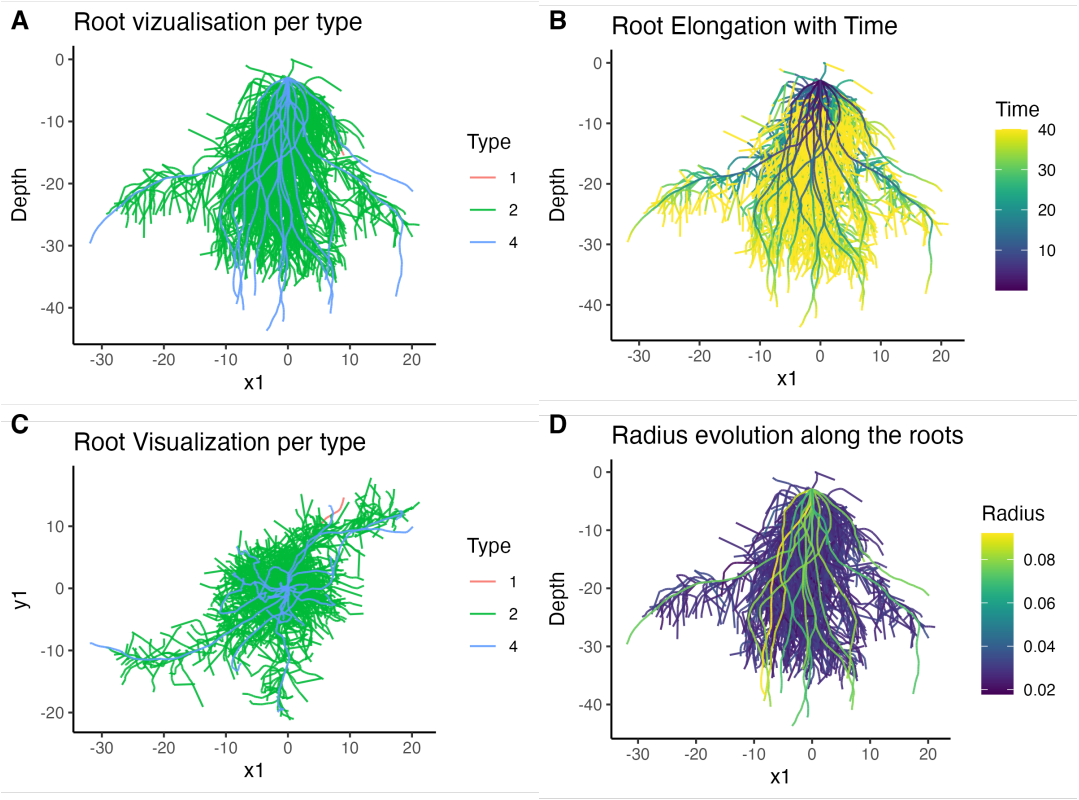

Figure 4.14: Root visualization for spelt after 40 days

Figure 4.15 illustrates the simulation of the evolution of a spelt root system with a five-day period between observations. As previously stated with regard to Rye and Oat, all of the main roots are formed within a five-day period following seeding. The emergence of the first laterals is observed on day 10, reaching their maximum length with minimal subsequent growth. It is noteworthy that the lateral roots are markedly less developed than those observed in the other two species.

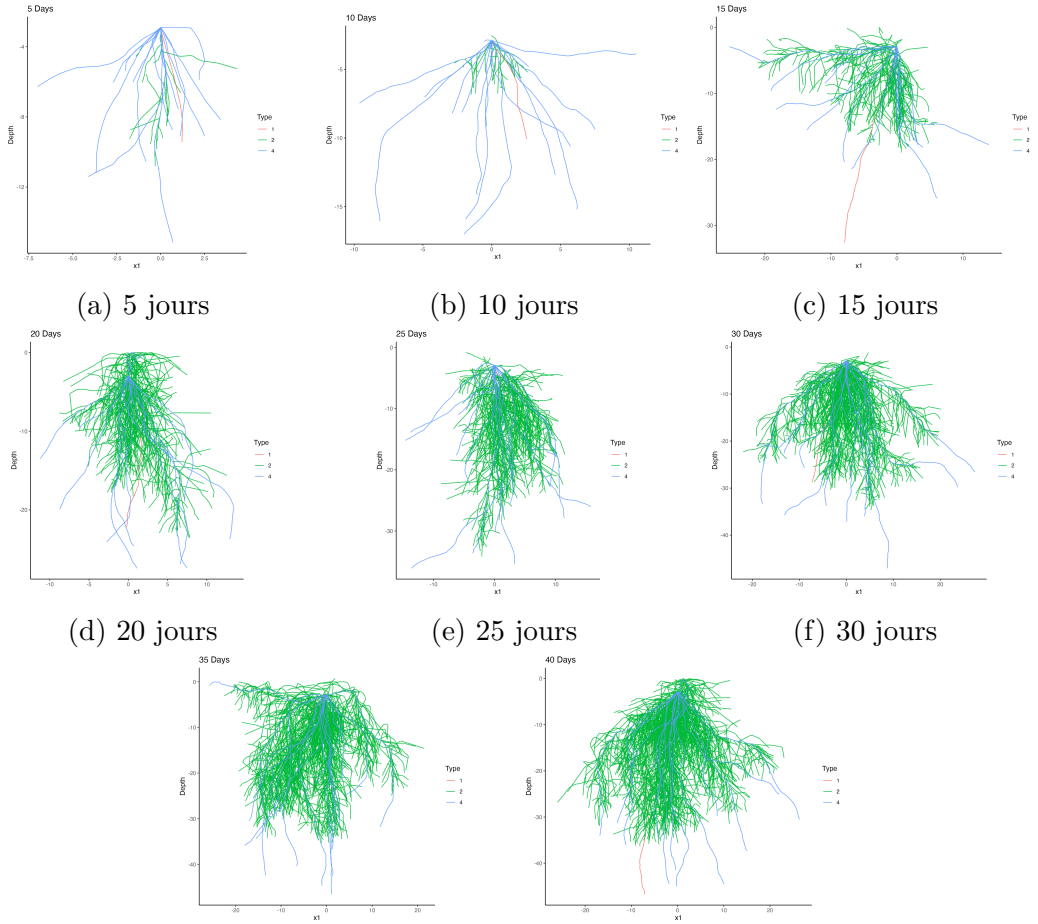

(a) 5 jours (b) 10 jours (c) 15 jours

(d) 20 jours (e) 25 jours (f) 30 jours

(g) 35 jours (h) 40 jours

Figure 4.15: Root visualization at 5 days interval for spelt

Figure 4.16a shows the evolution of root length by type. Just like for rye and oat, most of the contribution to this total length comes from the lateral roots.

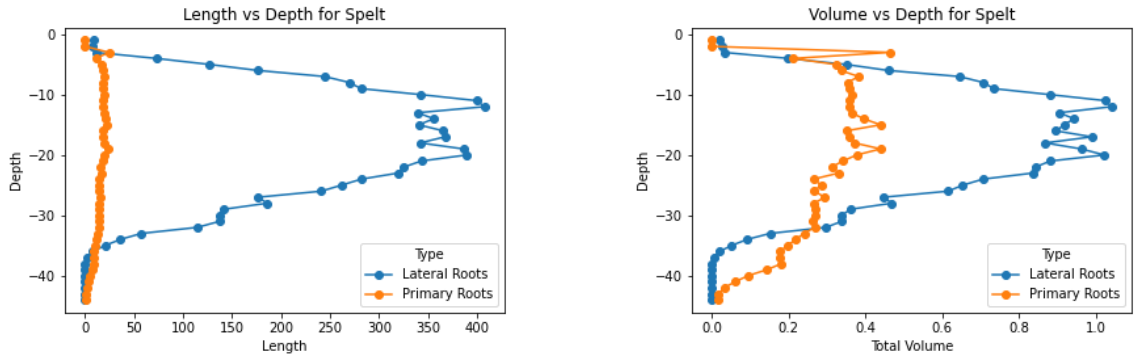

(a) Total Root length in function of depth for Spelt

(b) Total Volume of roots in function of depth for Spelt

Figure 4.16: Underground representation of the Spelt root system

Figure 4.16b shows that most of the roots volume is attributed to the lateral roots,

just like for oat. A notable distinction between the two is the considerably smaller root volume of spelt. This can be attributed to the fact that the radius of oat and spelt are similar. Table 4.37 corroborates our observations and the fact that their primary root volume is smaller.

Type	**Volume** (cm^3)	**Length(cm)**
Lateral Roots	20.739620	8025.4407
Primary Roots	11.590654	616.0542

Table 4.37: Sum of the volumes and length per root type for spelt

4.3.4 General results for CRootBox simulations

Table 4.38 presents a comprehensive overview of the general results obtained from the simulations. It is evident that rye exhibits the highest values across all parameters, with the exception of width and diameter. Spelt, which has the lowest values for each parameter, has the highest width. This is likely due to the fact that, given its shallower depth, it extends further across the width than its counterparts.

Parameter	**Spelt**	**Oat**	**Rye**
Tot_root_length (cm)	8641.495	9030.485	9765.897
Volume_tot (cm^3)	32.33027	42.16079	43.41343
Max_depth (cm)	-43.6962	-49.0002	-49.9672
Max_Width (cm)	53.1399	46.9115	47.0113
Mean_Diameter (cm)	0.06458038	0.0697638	0.06624141

Table 4.38: Results of the CRootBox simulation for the different species

4.4 RSHA simulations with Marshal

This section presents the results of the RSHA for each species using the MARSHAL macrohydraulic quantification tool. As a reminder, in order for MARSHAL to function, the following requirements must be met:

- The hydraulic properties of the roots (Figure 3.9 and 3.10)
- The water potential of the soil (Table 3.5)
- The RSA for each specie

- The initial pressure strength that pulls water out of the collar (Psi at the collar $=-15000\ hPa$)

The two characteristics, K_{rs} and SUF, are sufficient to describe the total uptake of the root system (Vanderborght et al., 2021). The root system conductance (K_{rs}) is a measure of the ease with which water can rise and be absorbed by roots. A higher conductance rate indicates that water can be absorbed from the soil with greater ease (Meunier et al., 2019). The standard uptake fraction (SUF) of a root is a critical factor in assessing the efficiency of water and nutrient uptake by plants. SUF represents the uptake from a soil profile with a uniform hydraulic head, indicating the proportion of available resources taken up by the roots annually (Vanderborght et al., 2021). The total of all root SUFs is equal to one, and the SUF of a root portion represents the contribution of that portion to the overall result. A root portion with a higher SUF is demonstrably more effective at absorbing water and nutrients than a portion with a lower SUF (Vanderborght et al., 2021).

In Table 4.39 we can find the results of macroscopic parameters after MARSHAL simulations. We can see that the values are of the same order of magnitude, for each parameter and for each species:

- K_{rs}: Oat have the highest conductance, with minimal differentiation from rye. Spelt has the lowest conductance, but the difference between it and the other two is minimal.

- With regard to the z_{SUF}, it represents the average depth where the contribution to water and nutrient uptake is the highest (Meunier et al., 2019). As previously noted, spelt has the greatest depth, but only by a single centimeter compared with the other two, which are not at all different. In fact, the difference between them is just one millimeter.

- **Potential transpiration** refers to the maximum transpiration that the root system is capable of achieving. In this instance, the most significant discrepancy is evident. It is evident that spelt has a maximum transpiration capacity that is approximately 100 $\mathbf{cm^3}$ less than that of rye and oat.

- **Actual transpiration** is defined as the transpiration obtained at time t with a given soil. In this instance, we have opted for a dry soil scenario (please refer to Figure 2 in the attached tabular presentation). Spelt has the lowest transpiration, which is in line with expectations given the maximum transpiration this species is capable of.

Parameter	**Spelt**	**Oat**	**Rye**
K_{rs} $[cm^4\ hPa^{-1}\ day^{-1}]$	0.02279	0.0289	0.0286
z_{SUF} $[cm]$	-9.273683	-8.381944	-8.391366
Potential transpiration $[cm^3\ plante^{-1}\ day^{-1}]$	335.11975	424.85113	421.06445
Actual transpiration $[cm^3\ plante^{-1}\ day^{-1}]$	42.2829	48.4503	48.0722

Table 4.39: MARSHAL results simulations for the different species

Figure 4.17 illustrates the position of SUF in relation to soil depth. This serves to corroborate the z_{SUF} calculations that were previously quoted. However, the data indicates that the vast majority of SUF are situated at depths exceeding 20 cm, which suggests that absorption efficiency is relatively close to the surface. There is not a significant difference between the species, although it is evident that spelt does not reach the same maximum SUF as rye and oat.

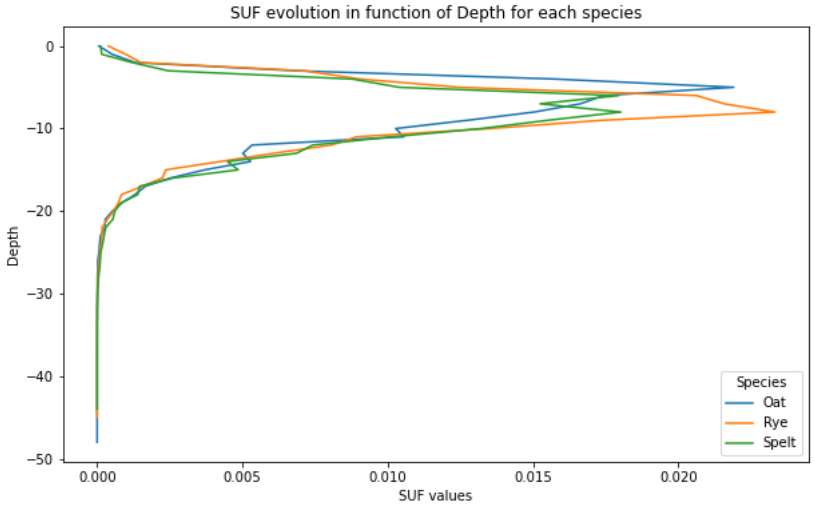

Figure 4.17: Root visualization for spelt after 40 days

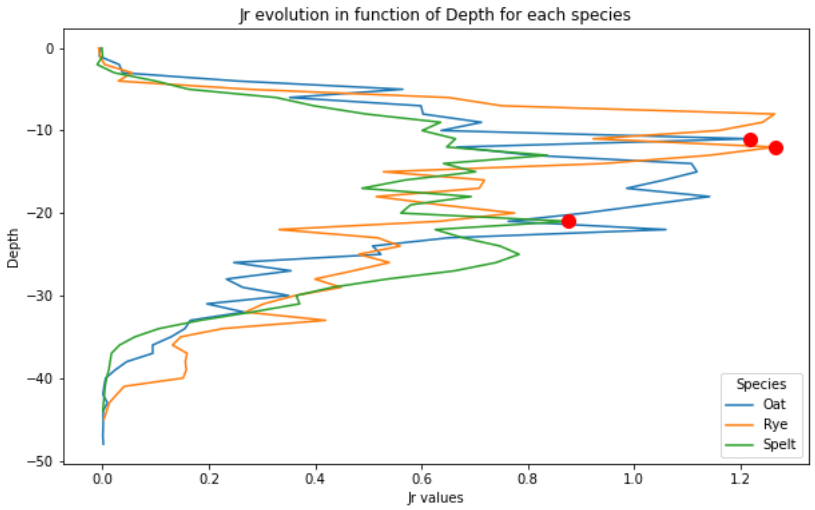

Figure 4.18: Root visualization for spelt after 40 days

Figure 4.18 illustrates the evolution of radial fluxes for each root segment as a function of depth. In this instance, the results are rather contrasting. The highest J_r values are indicated by a red dot on the graph. For rye and oat, the maximum values are nearly equivalent (1.21 and 1.26, respectively) and significantly lower for spelt (0.87). However, this deficit can potentially be offset by the fact that spelt maintains a fairly constant radial flow down to a depth of 25 cm. Oat sustain remarkably high J_r rates down to a depth of 20 cm. This stands in contrast to rye, which maintains high values over a comparatively less interval of depth.

CHAPTER 5

DISCUSSION

5.1 Results Discussion

5.1.1 Effect of the variety

Inter-variety comparisons within each species generally showed very few differences for each parameter. It should be noted, however, that for lateral root diameter, this was the only parameter for which comparisons within each species showed a difference between varieties, and for all varieties two to two. This may be due to the large sample sizes (of the order of 10,000 observations), which enabled more precise averages to be obtained and differences to be seen more easily. As far as primary root diameters are concerned, only Rye and Spelt showed differences in their average between varieties. In the case of spelt, this was mainly due to a significantly lower average for the *Epeautre Cosmos* variety.

It can be concluded that the variety effect did not play a role in the evaluation of the parameters, which is why simulations for each of the varieties were not run. It would be unwise, however, to claim that these varieties are identical. The evidence suggests that, in terms of the observed parameters, there are only a few differences between them.

5.1.2 Roots quantification

Dry weight

In terms of dry weight, the results demonstrated two distinct outcomes. In the rhizotron experiment, oat exhibited the highest dry weight, with a statistically significant difference from the other species. However, the column experiment indicated that rye exhibited the highest dry weight. Despite the disparate temporal and environmental parameters of the two experiments, the discrepancy in outcomes is noteworthy. It is not possible to draw any conclusions from this difference, as the growing conditions are highly atypical

for rhizotrons with Hoagland's solution. It may be that oat react much better to this solution. However, it should also be noted that dry weight values are much lower in rhizotrons. It is therefore probable that this experimental system is more restrictive for aerial growth, and no comparison is possible.

Roots part

Although some numerical values differ between parameters, it is not correct to conclude that one is better than the other on this basis alone. It is essential to refer to the ANOVA analyses, which show that only differences in lateral and main root diameters and in the number of main roots are significant between species. We can, however, discuss the comparison with the values for wheat taken from the study by Bingham and Wu (2011). In all cases, none of the values appear to be outliers compared with the wheat data. However, it is important to note that the comparison between our values and those for wheat is limited, as the data for wheat come from a field experiment (Bingham and Wu, 2011), involving plant competition in the soil as well as variable environmental conditions. Furthermore, it would be premature to draw conclusions at this stage, given that the number of samples is insufficient to allow for an optimal characterization of the parameters in question.

5.1.3 Model results for the cereals

First of all, there are a few problems with the simulations using the parameters from the Bingham and Wu (2011) study. We can start with the maximum length of the main roots. It is hard to believe that roots can have a maximum length of 60cm. As well as being debatable, this value also slows down the progression of the roots in the simulation, leaving us with almost identical values for depth, for example. Let's look at a new simulation with l_{max} 100cm (arbitrary upper value). You'll see that the values are much higher in every aspect. So it is important to set l_{max} to the correct value to get results that are closer to reality.

In addition, the main root emergence parameter is not optimal either. Being set to zero, it causes all the roots to emerge at once, whereas in reality the appearance of new roots is spaced out over time. It is therefore essential that the *delayB* parameter is adapted so that development is as realistic as possible and, for example, evolution every 5 days makes sense.

5.2 Comparison with wheat

To better assess the impact of root parameters, we can compare our results with a simulation for *Triticum aestivum* wheat (carried out using the parameters in Table 4.34). Although no major differences in root architecture are apparent, significant differences in the final statistics, presented in Table 5.1, are worth highlighting. Although the maximum depth and average diameter are almost equivalent, wheat has a much greater total root length and volume than our three species. This can be explained by a higher growth rate in wheat, which allows it to develop a greater number of roots, thus increasing its total length and volume.

Parameter	**Value**
Tot_root_length (cm)	20729.16
Volume_tot (cm^3)	62.64924
Max_depth (cm)	-49.2872
Max_Width (cm)	59.0008
Mean_Diameter (cm)	0.06258449

Table 5.1: Results of the CRootBox simulation for wheat

But, does-it have an impact on the RSHA properties ? Yes it does. In fact, as shown in the Table 5.2, the K_{rs} (water conductivity) as well as potential and actual transpiration increased compared with the other species. This suggests a causal link: wheat's greater root length and volume enable it to transpire more and improve its conductance, which is crucial in a dry environment. However, the optimum depth for capturing water and nutrients (z_{SUF}) is similar to that of rye and oat.

Parameter	**Spelt**
K_{rs} $[cm^4\ hPa^{-1}\ day^{-1}]$	0.03851
z_{SUF} $[cm]$	-8.433631
Potential transpiration $[cm^3\ plante^{-1}\ day^{-1}]$	566.103
Actual transpiration $[cm^3\ plante^{-1}\ day^{-1}]$	64.9567

Table 5.2: MARSHAL results simulations for wheat

Nevertheless, the presented results do not provide definitive evidence that wheat is a superior candidate for drought resistance. However, they do elucidate the influence of specific parameters on root architecture.

5.3 Areas for Improvement

It must be acknowledged that the work presented is not without flaws. In fact, the inclusion of a few approximations may have influenced the results obtained, resulting in a simulation that is significantly detached from reality.

Firstly, the selection of identical parameters for each species enables a comparison of species on a consistent basis, despite the absence of precise data. It is evident that this approximation results in a significant discrepancy between the presented results and the actual reality. Moreover, the three species exhibit strikingly similar architectural patterns, with the primary distinction lying in their macro-characteristics. However, this assertion is not supported by the visual evidence. To achieve ultra-realistic results, it would be necessary to collect a substantial number of additional parameters and identify alternative methods for doing so, beyond those employed in this study.

Moreover, the selection of hydraulic conductivities along the roots was based on a set of values derived from existing literature. However, these were adapted for a maize root system to enhance usability, as they were directly aligned with MARSHAL. While this approach enabled us to compare these species on a limited number of parameters, it would have been more appropriate to select a set of conductivities from wheat, or even more accurately, to utilize conductivities that had been adapted for each species. To obtain these conductivities, we should refer to Marco d'Agostino (2022)'s work, which enabled us to characterize root anatomy via cross-sections and transpose it into the GRANAR tool (Heymans et al., 2019), which models root anatomy. Once the requisite data has been obtained for GRANAR, they can be entered into MECHA, which will calculate the relevant hydraulic conductivities based on the provided anatomies. The collection of all these conductivities would undoubtedly have led to more realistic hydraulic results.

One potential parameter for analysis is the shoot-to-root ratio. The shoot-to-root ratio is typically calculated by dividing the biomass or length of the above-ground components of the plant by the biomass or length of the roots. This straightforward calculation offers a quantitative assessment of the distribution of biomass or growth between the aerial and root parts of the plant. Moreover, research has demonstrated that lower shoot-to-root ratios are correlated with enhanced adaptation to water stress in certain plant species (Graves, 1994). This may reflect a greater allocation of resources to the roots, thereby enhancing water uptake and plant survival under adverse environmental conditions (Misra et al., 1997)). The literature indicates that for rye, the ratio is 4 when the plant is sown indoors and 5 outdoors at anthesis (Sheng and Hunt, 1991). In the same study, rye root growth surpassed all the others (wheat and triticale) after anthesis, and root dry weight was greater at final harvest. In the case of oat, as indicated by Bolinder et al. (1997), the

SR estimation provides a ratio of 2.5, which is markedly disparate from that of winter wheat and barley on the identical analysis site. The ratio at maturity for wheat is the greatest, while that for barley is the least. No ratio values could be identified for spelt. However, according to Akman (2017), with respect to root/shoot and root/total biomass ratio, Triticum spelta exhibits a higher value than the other species that were studied (ancient and modern wheat species). The study concludes that Triticum spelta may be evaluated for new, improved cultivars with greater tolerance to water stress factors in breeding programs.

The absence of field or experimental data to validate the results presented herein renders further in-depth analysis and the drawing of solid conclusions challenging.

5.4 Future Perspectives

Understanding the system's architecture and hydraulic capabilities are just some of the steps involved in understanding the impact of these flows on crop growth and biomass production. The pipeline between CRootBox and MARSHAL is fairly intuitive, and it is very easy to pass outputs from one to the other without much data manipulation. However, an additional interesting pipeline can be realized between CRootBox, MARSHAL and APSIM (Holzworth et al., 2014), which is a model for predicting crop water dynamics and biomass growth and production, or any other model that models crops. Coupling can take place either via K_{rs} or via transpiration. Being able to couple all this can therefore prove interesting for getting an overview and making yield predictions for different scenarios as well as for an immense number of different species, which is a crucial step in simulating cultivars adapted to the climate changes to come in the next few years.

SmartRoot is a wonderful, intuitive tool for manually and accurately tracing roots. However, it is very time consuming. Can it be replaced by its time-saving counterpart, Rhizovision (Seethepalli et al., 2021)? It is true that Rhizovision saves time and increases efficiency and ease of harvesting due to its automatic operation. However, this is not to be taken lightly, as each of these programs has its own strengths and weaknesses. Rhizovision offers a comprehensive set of measurements related to root morphology and geometry, including width-to-depth ratio, network area, and perimeter. While this tool enhances our visualization of root structure, it does not provide detailed information on individual root characteristics. Conversely, SmartRoot is particularly adept at examining the attributes and progression of individual roots. The CSV output is more readily manipulable, facilitating the derivation of the requisite parameters for the model. The combination of the two software packages offers an opportunity to gain a comprehensive understanding of root structure, morphology, and development on a global scale Mariam (2024).

CONCLUSION

This research contributes to a larger study focused on understanding the internal water dynamics in plants. The main goal is to identify crop varieties and genetic traits that improve resilience to frequent droughts, helping in the selection of more robust varieties and genetic profiles. In the past, studies have concentrated on the above-ground parts of plants for the purpose of selection, given the inherent difficulties in sampling the roots parts. While a great deal of knowledge has been accumulated regarding individual processes, a comprehensive and accurate description of root systems as a whole remains elusive.

Rye, oat, and spelt are well-established cereals in our agricultural regions. They are related to wheat in their ability to till. These cereals are integral to certain foods, so it is crucial to assess their resilience to more intense droughts due to global warming. However, there is limited information about their root morphology. Therefore, a modeling approach is essential to prepare for the future.

The study focused on three varieties of each species: Oat Jacky (AJ), Oat KWS Opaline (AO), Oat Lion (AL), Rye KWS Serafino (SS), Rye Tayo (ST), Rye Poséidon (SP), Spelt Cosmos (EC), Spelt Sérénité (ES) and Spelt Zollernspelz (EZ). These 9 varieties are currently grown by the majority of Walloon growers. They have therefore been tested in rhizotrons as well as in columns.

First, the root systems were quantified. 5 parameters were chosen (Dprimary, Dlateral, IBD, Growth rate and Number of root axes). Coming from these parameters, statistics analysis have been pursued and showed that for three parameters, the differences between species have been noticed. De ces paramrètres des analyses statistiques ont été développées et ont montré que pour 3 de ces paramètres, les différences entre les espèces étaient inhérrentes.

Based on these average estimates, root system simulations were carried out using the CRooBox tool. This revealed some differences in the statistics, but the architectures themselves were similar. This is probably due to the fact that most of the parameters used for CRootBox were the same for all three species. In addition, analyses of the hydraulic architectures of these simulated root systems were carried out using the MARSHAL model. Very few differences were observed, apart from transpiration and Ks for spelt, which is potentially weaker under drought conditions than its congeners. A comparison with wheat was also conducted and showed the importance of the parameters and their impact on the RSHA of each plant.

The next step of this master thesis is to use a crop model prediction like APSIM to predict the water dynamics within the soil and the plant and the biomass growth of the crop in order to make yield prediction. The other idea is to join the root system quantification of SmartRoot with also Rhizovision to include root morphology and geometry.

BIBLIOGRAPHY

Akman, H. (2017). Root Biomass Distribution with Root and Shoot Development at Different Growth Stages of Wild, Ancient and Modern Wheat Species. *Turkish Journal of Agriculture - Food Science and Technology*, 5(11):1422–1428.

Bingham, I. J. and Wu, L. (2011). Simulation of wheat growth using the 3d root architecture model spacsys: Validation and sensitivity analysis. *European Journal of Agronomy*, 34(3):181–189.

Bolinder, M., Angers, D., and Dubuc, J. (1997). Estimating shoot to root ratios and annual carbon inputs in soils for cereal crops. *Agriculture, Ecosystems & Environment*, 63(1):61–66.

Boote, K. J. (1976). Root:shoot relationships. *Soil Crop Sci. Soc. Fl. Proc*, 36:15–23.

Burgos, S., Stamp, P., and Schmid, J. E. (2001). Agronomic and physiological study of cold and flooding tolerance of spelt (triticum spelta l.) and wheat (triticum aestivum l.). *Journal of Agronomy and Crop Science*, 187(3):195–202.

Correa, J., Postma, J. A., Watt, M., and Wojciechowski, T. (2019). Soil compaction and the architectural plasticity of root systems. *Journal of Experimental Botany*, 70(21):6019–6034.

Couvreur, V., Faget, M., Lobet, G., Javaux, M., Chaumont, F., and Draye, X. (2018). Going with the Flow: Multiscale Insights into the Composite Nature of Water Transport in Roots. *Plant Physiology*, 178(4):1689–1703.

Couvreur, V., Vanderborght, J., and Javaux, M. (2012). A simple three-dimensional macroscopic root water uptake model based on the hydraulic architecture approach. *Hydrology and Earth System Sciences*, 16(8):2957–2971.

d'Agostino, M. (2022). How do root anatomy influences water uptake in tomato ? updates of protocols and computational tools for the characterization of tomato root anatomy. Master's thesis, UCLouvain.

Del Bianco, M. and Kepinski, S. (2018). Building a future with root architecture. *Journal of Experimental Botany*, 69(22):5319–5323.

Dixon, H. H. (1894). On the ascent of sap. *Annals of Botany*, os-8:468–470.

Doussan, C. (1998). Modelling of the Hydraulic Architecture of Root Systems: An Integrated Approach to Water Absorption—Distribution of Axial and Radial Conductances in Maize. *Annals of Botany*, 81(2):225–232.

Dreyer, H. (2018). 2) review and amend, as needed, the Draft Conference Resolution presented in Appendix A, and submit it for consideration of and adoption by the 41st Session of the Conference (22-29 June 2019). *FAO*.

Eremina, D. (2021). The influence of mineral fertilizers on the mass of plant-root residues of grain crops on chernozem soils of the western siberia. *Bio Web of Conferences*, 36:03007.

Fernando, K. M. C., Wibowo, C., and Sparkes, D. L. (2021). Genotypic dependence of wheat species in nitrogen uptake determines by root morphology at maturity. *Tropical Agricultural Research and Extension*, 24(2):92.

Frensch, J. and Steudle, E. (1989). Axial and Radial Hydraulic Resistance to Roots of Maize (Zea mays L.) 1. *Plant Physiology*, 91(2):719–726.

Geiger, H. and Miedaner, T. (2009). Rye (secale cereale l.). In Carena, M. J., editor, *Cereals*, pages 157–181. Springer US, New York, NY.

Graves, W. R. (1994). Seedling development of sugar maple and black maple irrigated at various frequencies. *Hortscience*.

Graw-Hill, M. (2002). McGraw-Hill dictionary of scientific and technical terms (6e édition). *McGraw*.

Heymans, A., Couvreur, V., LaRue, T., Paez-Garcia, A., and Lobet, G. (2019). GRANAR, a Computational Tool to Better Understand the Functional Importance of Monocotyledon Root Anatomy1 [OPEN]. *Plant Physiology*, 182(2):707–720.

Heymans, A., Meunier, F., and Lobet, G. (2018). Getting a Functionnal-Structural Plant Model into a comprehensive R pipeline:.

Holzworth, D. P., Huth, N. I., deVoil, P. G., Zurcher, E. J., Herrmann, N. I., McLean, G., Chenu, K., van Oosterom, E. J., Snow, V., Murphy, C., Moore, A. D., Brown, H., Whish, J. P., Verrall, S., Fainges, J., Bell, L. W., Peake, A. S., Poulton, P. L., Hochman, Z., Thorburn, P. J., Gaydon, D. S., Dalgliesh, N. P., Rodriguez, D., Cox, H., Chapman, S., Doherty, A., Teixeira, E., Sharp, J., Cichota, R., Vogeler, I., Li, F. Y., Wang, E., Hammer, G. L., Robertson, M. J., Dimes, J. P., Whitbread, A. M., Hunt, J., van Rees, H., McClelland, T., Carberry, P. S., Hargreaves, J. N., MacLeod, N., McDonald, C., Harsdorf, J., Wedgwood, S., and Keating, B. A. (2014). Apsim – evolution towards a new generation of agricultural systems simulation. *Environmental Modelling & Software*, 62:327–350.

Jong Un, C. (1993). Variations in rate of leaf emergence, initiation of ear primordium, stem elongation and heading time as affected by vernalization duration of barley with differing growth habits. *Field Crops Research*, 32(1):159–172.

Khan, T. A. (2019). A larger root system in oat (avena nuda l.) is coupled with enhanced biomass accumulation and hormonal alterations under low nitrogen. *Applied Ecology and Environmental Research*, 17:4631–4653.

Kim, Y. X., Ranathunge, K., Lee, S., Lee, Y., Lee, D., and Sung, J. (2018). Composite Transport Model and Water and Solute Transport across Plant Roots: An Update. *Frontiers in Plant Science*, 9:193.

Leitner, D., Klepsch, S., Bodner, G., and Schnepf, A. (2010). A dynamic root system growth model based on L-Systems: Tropisms and coupling to nutrient uptake from soil. *Plant and Soil*, 332(1-2):177–192.

Liu, X. (2023). Root architecture of forage species varies with intercropping combinations. *Agronomy*, 13:2223.

Lobet, G., Couvreur, V., Meunier, F., Javaux, M., and Draye, X. (2014). Plant Water Uptake in Drying Soils. *Plant Physiology*, 164(4):1619–1627.

Lobet, G., Koevoets, I., Noll, M., Meyer, P., Tocquin, P., Pagès, L., and Périlleux, C. (2017). Using a structural root system model to evaluate and improve the accuracy of root image analysis pipelines. *Frontiers in Plant Science*, 8.

Lobet, G., Pagès, L., and Draye, X. (2011). A Novel Image-Analysis Toolbox Enabling Quantitative Analysis of Root System Architecture . *Plant Physiology*, 157(1):29–39.

Lobet, G., Pound, M. P., Diener, J., Pradal, C., Draye, X., Godin, C., Javaux, M., Leitner, D., Meunier, F., Nacry, P., Pridmore, T. P., and Schnepf, A. (2015). Root System Markup Language: Toward a Unified Root Architecture Description Language. *Plant Physiology*, 167(3):617–627.

Lynch, J. P. (2013). Steep, cheap and deep: an ideotype to optimize water and N acquisition by maize root systems. *Annals of Botany*, 112(2):347–357.

Lynch, J. P., Chimungu, J. G., and Brown, K. M. (2014). Root anatomical phenes associated with water acquisition from drying soil: targets for crop improvement. *Journal of Experimental Botany*, 65(21):6155–6166.

Lynch, J. P., Nielsen, K. L., Davis, R. D., and Jablokow, A. G. (1997). Simroot: Modelling and visualization of root systems. *Plant and Soil*, 188(1):139–151.

Mariam, K. (2024). Quantification of plant root architecture: development of an integrated experiment-to-model pipeline. Master's thesis, UCLouvain.

Martin, M. and Field, R. (1987). Competition between vegetative plants of wild oat (avena fatua l.) and wheat (triticum aestivum l.). *Weed Research*, 27:119–124.

Martin, M. P. L. D. and Field, R. J. (1988). Influence of time of emergence of wild oat on competition with wheat. *Weed Research*, 28:111–116.

Meier, U., Bleiholder, H., Buhr, L., Feller, C., Hack, H., Heß, M., Lancashire, P., Schnock, U., Stauß, R., Boom, T., Weber, E., and Zwerger, P. (2009). The bbch system to coding the phenological growth stages of plants-history and publications. *Journal für Kulturpflanzen*, 61:41–52.

Meunier, F., Draye, X., Vanderborght, J., Javaux, M., and Couvreur, V. (2017). A hybrid analytical-numerical method for solving water flow equations in root hydraulic architectures. *Applied Mathematical Modelling*, 52:648–663.

Meunier, F., Heymans, A., Draye, X., Couvreur, V., Javaux, M., and Lobet, G. (2019). MARSHAL, a novel tool for virtual phenotyping of maize root system hydraulic architectures. *in silico Plants*.

Misra, A. N., Sahu, S. M., Meera, I., Mohapatra, P. K., Das, N. K., and Misra, M. (1997). Root growth of a salt susceptible and a salt resistant rice (¡i¿oryza sativa¡/i¿ l.) during seedling establishment under nacl salinity. *Journal of Agronomy and Crop Science*.

Nagwa (2024). Fiche explicative de la leçon: Circulation dans le xylème. Accessed: July 25, 2024.

Ndour, A., Vadez, V., Pradal, C., and Lucas, M. (2017). Virtual Plants Need Water Too: Functional-Structural Root System Models in the Context of Drought Tolerance Breeding. *Front. Plant Sci.*, 8:1577.

Pagès, L., Bécel, C., Boukcim, H., Moreau, D., Nguyen, C., and Voisin, A.-S. (2014a). Calibration and evaluation of ArchiSimple, a simple model of root system architecture. *Ecol. Modell.*, 290:76–84.

Pagès, L., Bécel, C., Boukcim, H., Moreau, D., Nguyen, C., and Voisin, A.-S. (2014b). Calibration and evaluation of archisimple, a simple model of root system architecture. *Ecological Modelling*, 290:76–84. Special Issue of the 4th International Symposium on Plant Growth Modeling, Simulation, Visualization and Applications (PMA'12).

Pagès, L., Serra, V., Draye, X., Doussan, C., and Pierret, A. (2010). Estimating root elongation rates from morphological measurements of the root tip. *Plant and Soil*, 328(1-2):35–44.

Passot, S., Couvreur, V., Meunier, F., Draye, X., Javaux, M., Leitner, D., Pagès, L., Schnepf, A., Vanderborght, J., and Lobet, G. (2019). Connecting the dots between computational tools to analyse soil–root water relations. *Journal of Experimental Botany*, 70(9):2345–2357.

Passot, S., Gnacko, F., Moukouanga, D., Lucas, M., Guyomarc'H, S., Ortega, B., Atkinson, J., Belko, M., Bennett, M., Gantet, P., Wells, D., Guédon, Y., Vigouroux, Y., Verdeil, J.-L., Muller, B., and Laplaze, L. (2016). Characterization of pearl millet root architecture and anatomy reveals three types of lateral roots. *Frontiers in Plant Science*, 7.

Postma, J. A., Kuppe, C., Owen, M. R., Mellor, N., Griffiths, M., Bennett, M. J., Lynch, J. P., and Watt, M. (2017). OpenSimRoot: widening the scope and application of root architectural models. *New Phytol.*

Postma, J. A. and Lynch, J. P. (2011). Root Cortical Aerenchyma Enhances the Growth of Maize on Soils with Suboptimal Availability of Nitrogen, Phosphorus, and Potassium. *Plant Physiology*, 156(3):1190–1201.

Roose, T. and Fowler, A. (2004). A model for water uptake by plant roots. *Journal of Theoretical Biology*, 228(2):155–171.

Roychoudhry, S. and Kepinski, S. (2021). Auxin in Root Development. *Cold Spring Harbor Perspectives in Biology*, page a039933.

Schnepf, A., Leitner, D., Landl, M., Lobet, G., Mai, T. H., Morandage, S., Sheng, C., Zörner, M., Vanderborght, J., and Vereecken, H. (2018). CRootBox: a structural–functional modelling framework for root systems. *Ann. Bot.*, 121(5):1033–1053. Publisher: Oxford Academic.

Seethepalli, A., Dhakal, K., Griffiths, M., Guo, H., Freschet, G. T., and York, L. M. (2021). RhizoVision Explorer: open-source software for root image analysis and measurement standardization. *AoB PLANTS*, 13(6):plab056.

Sheng, Q. and Hunt, L. A. (1991). Shoot and root dry weight and soil water in wheat, triticale and rye. *Canadian Journal of Plant Science*, 71(1):41–49.

Steffens, B. and Rasmussen, A. (2016). The Physiology of Adventitious Roots. *Plant Physiology*, 170(2):603–617.

Steudle, E., Murrmann, M., and Peterson, C. A. (1993). Transport of Water and Solutes across Maize Roots Modified by Puncturing the Endodermis (Further Evidence for the Composite Transport Model of the Root). *Plant Physiology*, 103(2):335–349.

Sultan, B., Roudier, P., Quirion, P., Alhassane, A., Muller, B., Dingkuhn, M., Ciais, P., Guimberteau, M., Traore, S., and Baron, C. (2013). Assessing climate change impacts on sorghum and millet yields in the Sudanian and Sahelian savannas of West Africa. *Environmental Research Letters*, 8(1):014040.

Thaler, P. and Pagès, L. (1998). Modelling the influence of assimilate availability on root growth and architecture. *Plant and Soil*, 201(2):307–320.

Vanderborght, J., Couvreur, V., Meunier, F., Schnepf, A., Vereecken, H., Bouda, M., and Javaux, M. (2021). From hydraulic root architecture models to macroscopic representations of root hydraulics in soil water flow and land surface models. *Hydrology and Earth System Sciences*, 25(9):4835–4860.

Vinutha, H. P., Poornima, B., and Sagar, B. M. (2018). Detection of outliers using interquartile range technique from intrusion dataset. In Satapathy, S. C., Tavares, J. M. R., Bhateja, V., and Mohanty, J. R., editors, *Information and Decision Sciences*, pages 511–518, Singapore. Springer Singapore.

Wang, J., Baranski, M., Korkut, R., Kalee, H. A., Wood, L., Bilsborrow, P., Janovska, D., Leifert, A., Winter, S., Willson, A., Barkla, B., Leifert, C., Rempelos, L., and Volakakis, N. (2021). Performance of modern and traditional spelt wheat (triticum spelta) varieties in rain-fed and irrigated, organic and conventional production systems in a semi-arid environment; results from exploratory field experiments in crete, greece. *Agronomy*, 11(5).

Wasson, A. P., Richards, R. A., Chatrath, R., Misra, S. C., Prasad, S. V. S., Rebetzke, G. J., Kirkegaard, J. A., Christopher, J., and Watt, M. (2012). Traits and selection strategies to improve root systems and water uptake in water-limited wheat crops. *J. Exp. Bot.*, 63(9):3485–3498.

Yasrab, R., Atkinson, J., Wells, D., French, A., Pridmore, T., and Pound, M. (2019). Rootnav 2.0: deep learning for automatic navigation of complex plant root architectures. *Gigascience*, 8.

Yasrab, R., Mp, P., Ap, F., and Tp, P. (2020). Rootnet: a convolutional neural networks for complex plant root phenotyping from high-definition datasets. *bioRxiv*.

Zhu, J., Brown, K. M., and Lynch, J. P. (2010). Root cortical aerenchyma improves the drought tolerance of maize (*Zea mays* L.). *Plant, Cell & Environment*, 33(5):740–749.

Zobel, R. and Waisel, Y. (2009). Report of the Nomenclature Workgroup from ISRR V, Reprise.

Żabiński, Andrzej and Sadowska, Urszula (2018). Root system architecture in winter varieties of spelt (triticumspelta l.). *BIO Web Conf.*, 10:01019.

Appendices

APPENDIX A

HOAGLAND SOLUTION

Réactifs		Solution mère		Solution fille		
Composants	M.M (g/mol)	[C] (M)	[C] (g/L)	V/L (ml)	V/25L (ml)	[C] finale dans 25L
KNO3	101,103	2	202	2,5	62,5	0,005
Ca(NO3) x 4H2O	236,15	2	236	2,5	62,5	0,005
MgSO4 X 7H2O	246,47	2	493	1	25	0,002
NH4NO3	80,04	1	80	1	25	0,002
Minors :						
H3BO3	61,83	0,0463	2,86			0,000046
MnCl2 X 4H2O	197,91	0,0091	1,81			0,000091
ZnSO4 X 7H2O	287,56	0,0008	0,22	1	25	0,00000076
CuSO4 X 5H2O	249,69	0,0002	0,051			0,00000031
H3MoO4 X H2O or Na2MoO4 x 2 H2O	180,97 241,95	0,0005 0,0005	0,09 0,12			0,00000049 0,00000049
KH2PO4 (pH to 6 with 3M KOH)	136,08	1	136	0,5	12,5	0,0005
C10H12N2FeNaO8	421,1	0,0356	15	3	75	0,0001068

Figure A.1: Hoagland solution composition by PEPA laboratory (Mariam, 2024)

APPENDIX B

EXAMPLE OF A RHIZOTRON LAYOUT

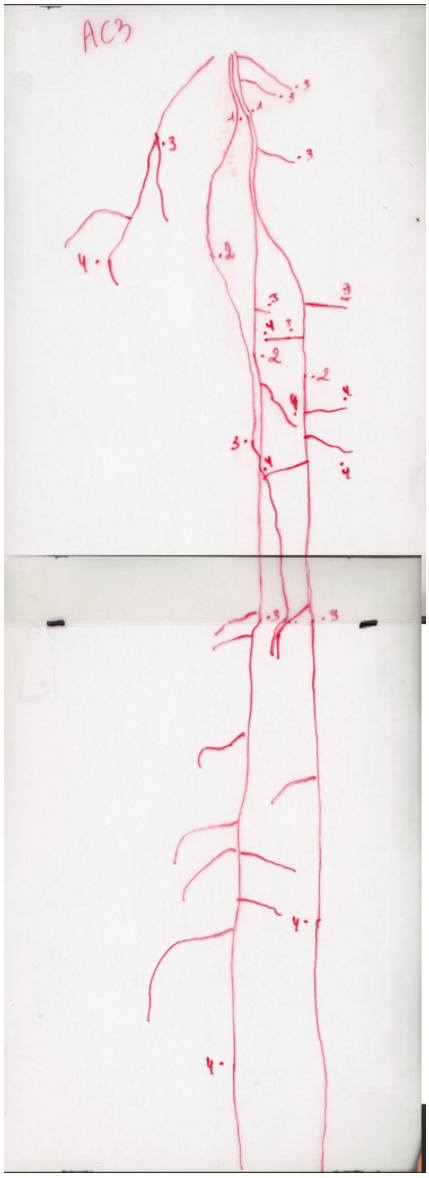

Figure B.1: Example of a rhizotron layout

APPENDIX C

SCANNER CONFIGURATION

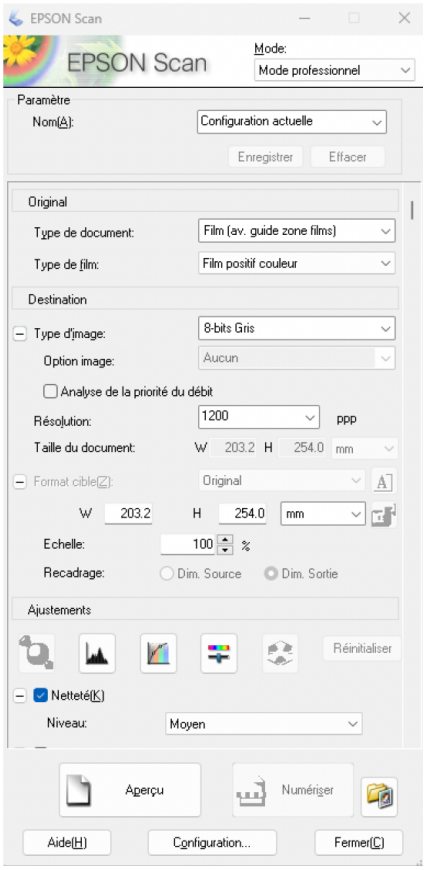

Figure C.1: Scanner Configuration

Quantification and characterization of Belgian cereals root system architecture and hydraulic architecture

Model-based approach

Pierre Huljev

Cereals represent the foundation of the global food supply, sustaining both animal and human diets. It is of the upmost importance to maintain this level of production to ensure the provision of sufficient food for the global population. However, the potential impact of global warming and the resulting increase in drought on food security can not be ignored. As a result, certain species may become less productive which could have serious consequences for global food security. Consequently, there is a growing interest in root systems, given that it is in the subsoil that nutrients and water are absorbed. Unfortunately, our understanding of the influence of root systems remains limited due to their hard sampling. However, our knowledge is evolving, and new techniques are becoming increasingly precise. More specifically, computational tools might help investigate the influence of architecture on water.

This work focused on characterizing the root and hydraulic architecture of 3 cereal species present in Belgium. 3 varieties for each species were taken from the CRA-W reserve. It highlighted the anatomical differences between these species on the basis of previously selected parameters. Based on the values of these parameters, root architectures could be simulated using the CRootBox model. They turned out to be very similar, because many of the parameters used were common to all 3 species. As for the hydraulic results, it was determined that compared with the other 2, spelt is the species with the least potential of the 3 to withstand drought.

To make these resutls realistic, many improvements are needed to be: taking more root parameters specific to these species and determining hydraulic conductivities using cross-sections. The next steps are to be able to couple these results with a crop prediction model and to be able to simulate the yield of these plants under certain soil and weather conditions.

UNIVERSITÉ CATHOLIQUE DE LOUVAIN
Faculté des bioingénieurs
Croix du Sud, 2 bte L7.05.01, 1348 Louvain-la-Neuve, Belgique | **www.uclouvain.be/agro**